T.R.
GEBZE TECHNICAL UNIVERSITY
GRADUATE SCHOOL OF NATURAL AND APPLIED SCIENCES

SIMULATION OF THE FLIGHT ANATOMY OF BIRDS WITH COMPUTATIONAL FLUID DYNAMICS

FERİT YILDIZ
A THESIS SUBMITTED FOR THE DEGREE OF
MASTER OF SCIENCE
DEPARTMENT OF MECHANICAL ENGINEERING

GEBZE
2020

T.R.

GEBZE TECHNICAL UNIVERSITY

GRADUATE SCHOOL OF NATURAL AND APPLIED SCIENCES

SIMULATION OF THE FLIGHT ANATOMY OF BIRDS WITH COMPUTATIONAL FLUID DYNAMICS

FERİT YILDIZ

A THESIS SUBMITTED FOR THE DEGREE OF

MASTER OF SCIENCE

DEPARTMENT OF MECHANICAL ENGINEERING

THESIS SUPERVISOR

ASSIST. PROF. DR. SEDAT TOKGÖZ

GEBZE

2020

T.C.
GEBZE TEKNİK ÜNİVERSİTESİ
FEN BİLİMLERİ ENSTİTÜSÜ

HESAPLAMALI AKIŞKANLAR DİNAMİĞİYLE KUŞLARIN UÇUŞ ANATOMİSİNİN SİMÜLASYONU

FERİT YILDIZ
YÜKSEK LİSANS TEZİ
MAKİNE MÜHENDİSLİĞİ ANABİLİM DALI

DANIŞMANI
DR. ÖĞR. ÜYESİ SEDAT TOKGÖZ

GEBZE
2020

GEBZE TEKNİK ÜNİVERSİTESİ	YÜKSEK LİSANS JÜRİ ONAY FORMU

GTÜ Fen Bilimleri Enstitüsü Yönetim Kurulu'nun 29/01/2020 tarih ve 2020/07 sayılı kararıyla oluşturulan jüri tarafından 14/05/2020 tarihinde tez savunma sınavı yapılan Ferit YILDIZ'ın tez çalışması Makine Mühendisliği Anabilim Dalında YÜKSEK LİSANS tezi olarak kabul edilmiştir.

JÜRİ

ÜYE
(TEZ DANIŞMANI) : DR. ÖĞR. ÜYESİ SEDAT TOKGÖZ

ÜYE : PROF. DR. İLYAS KANDEMİR

ÜYE : PROF. DR. CENK ÇELİK

ONAY

Gebze Teknik Üniversitesi Fen Bilimleri Enstitüsü Yönetim Kurulu'nun ...../...../..... tarih ve ...../..... sayılı kararı.

İMZA/MÜHÜR

SUMMARY

In this study, the flight behaviour of specially selected birds, which are known for their nearly silent flight types, are numerically analyzed in Computational Fluid Dynamics. The aim of this study is to investigate the low noise flight of the three bird profiles, and to show the aerodynamic effects of the owl airfoil compared to the falcon and the gull. The analysis are based on the angle of attack, the free stream velocity (flight speed) and acoustic features of the selected birds, while the bird wing cross sections are modelled according to their natural anatomy. The analysis are carried out numerically in a CFD software with suitable turbulence models for this work, where the acoustic model is chosen as the Ffowcs-Willams & Hawkings analogy. The aerodynamic effects on the acoustic is compared in terms of pressure, velocity, vorticity and sound pressure level, where the frequency interval for the acoustic data is set to 0-7500Hz. It was seen that the vorticity results are related to the acoustic results, and the owl showed the most silent flight among the three birds, especially between 0-3000Hz range. The falcon airfoil showed rather an average acoustic performance compared to the other two birds, while the gull airfoil took the lead in some regions in the frequency range above 3000Hz. It can be stated the effect of the owl airfoil shape ensured a relatively silent flight.

Key Words: Aerodynamics, Airfoil, Biological Flow, Bird Anatomy, Computational Fluid Dynamics.

ÖZET

Bu çalışmada, neredeyse sessiz uçuş tipleri ile bilinen, özel olarak seçilmiş kuşların uçuş davranışları, hesaplamalı akışkanlar dinamiği'nde sayısal olarak analiz edilmiştir. Bu çalışmanın amacı, üç kuş profilinin düşük gürültülü uçuşunu araştırmak ve baykuş kanat profilinin, şahin ve martı kanat profilleri ile karşılaştırıldığında aerodinamik etkilerini göstermektir. Analizler, hücum açısı, serbest akış hızı (uçuş hızı) ve seçilen kuşların akustik özelliklerine dayanırken, kuş kanadı kesitleri doğal anatomilerine göre modellenmiştir. Analizler, bu çalışma için uygun türbülans modellerine sahip bir hesaplamalı akışkanlar dinamiği yazılımında sayısal olarak gerçekleştirilmiştir. Bu çalışmada akustik model olarak Ffowcs-Willams & Hawkings yaklaşımı seçilmiştir. Akustik özellikler üzerindeki aerodinamik etkiler; basınç, hız, girdap ve ses basıncı seviyesi açısından karşılaştırılmıştır. Akustik veriler için frekans aralığı 0-7500Hz olarak belirlenmiştir. Bu çalışmada, vortisite sonuçlarının, akustik sonuçlarla ilişkili olduğu ve baykuşun, özellikle 0-3000Hz aralığında üç kuş arasında en sessiz uçuşa sahip olduğu görülmüştür. Şahin kanat profilinin, diğer iki kuşla karşılaştırıldığında ortalama bir akustik performans gösterirken, martı kanat profili, 3000Hz üzerindeki frekans aralığındaki bazı bölgelerde üstünlük sağlamıştır. Baykuş kanat profil geometrisinin, sessiz bir uçuşa nispeten olumlu bir etki sağladığı ifade edilebilir.

Anahtar Kelimeler: Aerodinamik, Biyolojik Akış, Hesaplamalı Akışkanlar Dinamiği, Kanat profili, Kuş Anatomisi.

ACKNOWLEDGEMENTS

I would like to express my deep and sincere gratitude to my supervisor, Assist. Prof. Sedat TOKGÖZ, who not only shared his profound scientific knowledge with me but also taught me great lessons of life. His support, suggestions and encouragement gave me the drive and will to complete this work.

I would also like to extend my deepest gratitude to Prof. Dr. Cenk ÇELİK for his knowledge, motivation, kindness and support throughout the study.

I wish to express my warm and sincere thanks to Umut Serdar ÇİVİCİ, Özgür ÇELEBİ and Anılcan TÜRKMEN for their collaboration to this research.

Finally, I am grateful to my family for their love and support.

TABLE of CONTENTS

	Page
SUMMARY	v
ÖZET	vi
ACKNOWLEDMENTS	vii
TABLE of CONTENTS	viii
LIST of FIGURES	x
LIST of TABLES	xiii
1. INTRODUCTION	1
1.1. Inspiration of Birds	1
1.2. Fundamentals of Birds	3
2. THEORETICAL BACKROUND, NUMERICAL SET-UP AND DESIGN	10
2.1. Aerodynamic – Sound Relation	10
2.1.1. Bird Flights Researches	17
2.2. Computational Details	20
2.2.1. Turbulence Model	20
2.2.2. Acoustic Model	22
2.3. 2D Design, Mesh and Setup	23
2.3.1. 2D Design	23
2.3.2. Mesh	25
2.3.3. Setup	26
3. RESULTS	28
3.1. Steady State Results	28
3.1.1. Pressure Distributions	28
3.1.2. Velocity Distributions	30
3.1.3. Vorticity Distributions	33
3.2. Transient Results	35
3.2.1. Owl	35
3.2.2. Falcon	38
3.2.3. Gull	41
3.2.4. Summary of the Results	44
4. ACOUSTIC RESULTS	47

4.1. Acoustic Results at the 0° Receiver 48
4.2. Acoustic Results for 360° Receiver Arrangement 51
5. CONCLUSION 57

REFERENCES 59
BIOGRAPHY 65
APPENDICES 66

LIST of FIGURES

Figure No:		Page
1.1:	a) Owl – b) Falcon – c) Seagull.	3
1.2:	Anatomy of a bird's wing.	5
1.3:	Barn Owl's wing.	5
1.4:	Seagull wing.	6
1.5:	Falcon wing.	6
1.6:	Wing adjustment of Seagulls a) one wing, b) both wings.	8
1.7:	Wing motion of a pigeon.	9
1.8:	Wing shape of a Falcon during a fast flight.	9
2.1:	Coefficient variation with angle of attack for an airfoil.	11
2.2:	2D Flow separation on an airfoil.	11
2.3:	Suction and pressure side on an airfoil. 1 and 2 are stagnation points.	12
2.4:	Flow types over a stationary wing profile at a low angle of attack under a horizontal flow.	12
2.5:	Kutta condition for different shapes of the trailing edge.	13
2.6:	Monopole and dipole examples.	15
2.7:	Streamlines of A) dipole source and B) vortices.	15
2.8:	Effect of velvet-like structure of Owl feathers on air flow. Serrations are breaking large turbulences down into small.	18
2.9:	Turbulence generation over a flate plate.	20
2.10:	2D profiles of a) owl, b) falcon, c) gull.	24
2.11:	Domain of airfoils.	25
2.12:	Mesh detail of airfoils.	26
3.1:	Absolute pressure contours for owl airfoil.	28
3.2:	Absolute pressure contours for falcon airfoil.	29
3.3:	Absolute pressure contours for gull airfoil.	30
3.4:	Velocity contours for owl airfoil.	31
3.5:	Velocity contours for falcon airfoil.	32
3.6:	Velocity contours for gull airfoil.	32
3.7:	Vorticity contours for owl airfoil.	33
3.8:	Vorticity contours for falcon airfoil.	34

3.9: Vorticity contours for gull airfoil. 35
3.10: Vorticity distributions of AOA=0° for owl airfoil in four equally spaced instants. 36
3.11: Vorticity distributions of AOA=5° for owl airfoil in four equally spaced instants. 37
3.12: Vorticity distributions of AOA=10° for owl airfoil in four equally spaced instants. 38
3.13: Vorticity distributions of AOA=0° for falcon airfoil in four equally spaced instants. 39
3.14: Vorticity distributions of AOA=5° for falcon airfoil in four equally spaced instants. 40
3.15: Vorticity distributions of AOA=10° for falcon airfoil in four equally spaced instants. 41
3.16: Vorticity distributions of AOA=0° for gull airfoil in four equally spaced instants. 42
3.17: Vorticity distributions of AOA=5° for gull airfoil in four equally spaced instants. 43
3.18: Vorticity distributions of AOA=10° for gull airfoil in four equally spaced instants. 44
3.19: Trailing edge vortex direction a) Owl (10°-10m/s), b) Falcon (10°-5m/s), c) Gull (10°-10m/s). The black arrows indicate the first movement of the streamlines just leaving the airfoil. 45
3.20: Vortex growth over the airfoil a) Owl (10°-10m/s), b) Falcon (10°-10m/s), c) Gull (10°-10m/s). 45
4.1: 360° receiver positions around airfoil. Each receiver is 1.5m away from the leading edge. 47
4.2: Sound pressure level between 0-7500 Hz for 5° AOA -5 m/s flow velocity. Receiver is located at the trailing edge (0°). Owl (purple), Falcon (green), Gull (black). 48
4.3: Sound pressure level between 0-7500 Hz for 5° AOA -10 m/s flow velocity. Receiver is located at the trailing edge (0°). Owl (purple), Falcon (green), Gull (black). 49

4.4: Sound pressure level between 0-7500 Hz for 10° AOA -5 m/s flow velocity. Receiver is located at the trailing edge (0°). Owl (purple), Falcon (green), Gull (black). 50
4.5: Sound pressure level between 0-7500 Hz for 10° AOA -10 m/s flow velocity. Receiver is located at the trailing edge (0°). Owl (purple), Falcon (green), Gull (black). 50
4.6: 360° OSPL distribution for Owl (green), Falcon (purple) and Gull (black). 18 receivers are equally placed around the airfoil. a) 5°AOA - 5 m/s, 20 – 120 Hz. b) 5°AOA - 10 m/s, 90 – 290 Hz. 52
4.7: 360° OSPL distribution for Owl (green), Falcon (purple) and Gull (black). 18 receivers are equally placed around the airfoil. a) 10°AOA - 5 m/s, 15 – 70 Hz. b) 10°AOA - 10 m/s, 40 – 170 Hz. 53
4.8: Vortex results in far-field for a) Gull AOA=10°-5 m/s, b) Gull AOA=10°-10 m/s, c) Gull AOA=5°-5 m/s, d) Gull AOA=5°-10 m/s, e) Owl AOA=10°-5 m/s, f) Falcon AOA=10°-5 m/s. The white point indicates to the 0° receiver at the trailing edge, where the black arrow shows the focusing direction of the long vortices. 54
4.9: 360° OSPL distribution for an interval of 300-750 Hz. a) AOA=10°-5 m/s results for Owl (green), Falcon (purple) and Gull (black), b) Results for Gull AOA=10°-5 m/s (black), AOA=10°-10 m/s (gray), AOA=5°-5 m/s (red), AOA=5°-10 m/s (blue). 55
4.10: 360° OSPL distribution for an interval of 900-1200 Hz. a) AOA=10°-5 m/s results for Owl (green), Falcon (purple) and Gull (black), b) Results for Gull AOA=10°-5 m/s (black), AOA=10°-10 m/s (gray), AOA=5°-5 m/s (red), AOA=5°-10 m/s (blue). 55

LIST of TABLES

Table No:	**Page**
2.1: Different chord lengths of owl, falcon and gull.	24

1. INTRODUCTION

Different solutions for low noise aircrafts can be found in industry. With this in mind, aircraftsman inspired by birds, which seek for solutions to aerodynamics and aeroacoustics of flight [20]. Following this, various properties of birds were implemented to aircraft designs, and it helped to develope aviation. Consequently, one of the best adaptation of these subjects probably lies in the nature itself. Birds, which are responsible for the desire of flying, are analyzed for further improvements in aviation [71]. Therefore, researchers went a step forth and developed new techniques with the help of nature to achieve new improvements in terms of aerodynamic and silent flight [24]. The scope of this thesis is to investigate low noise flight structures of specially selected birds which are known for their nearly silent flight types. Various aerodynamic properties like velocity contours or vortex formations were investigated to understand the noise generation of avians. Furthermore, the connection between these properties and acoustics were examined.

1.1. Inspiration of Birds

Flying animals were fascinating human beings for centuries. They observed the flight of birds and insects, and started to imitate the motions and structures. Examples can be given form the Greek story of an engineer Daedalus, who built wings of wax and feathers to help his son to escape from prison, or Leonardo DaVinci's sketches (codices) about flying machines, the nature of air, and bird flight [56]. Hezârfen Ahmed Çelebi, the legendary Ottoman aviator who used the Galata Tower as his departure point (located at the European side of Istanbul) and then arrives at the Anatolian side, Üsküdar. These are two example of legends that amply reflect our interest in flight dating back hundreds or thousands of years [79].

As understood from the paragraph above, engineers studied birds for inventing different aircrafts or at least developed new parts for aircrafts. By investigating various bird species, the distinction in flight kinematics and aerodynamics were understood and categorized over time. This led to diverse types of aircrafts, which served for different purposes. For example, gliding capabilities lead to fuel saving, wing or body shapes to variable speed flight and wing kinematics to exceptional maneuvering [20].

Within the years, humans developed highly advanced aircrafts which based on special bird parts [56].

Every challenge created a new level in design, control, material, structure, fuel etc. Apart from these topics, our scope was turned to acoustics or noise generation during flight. As mentioned in the previous section, the birds can provide a lot of details in terms of aviation. Especially by focusing on acoustics, only a few animals are coupled with the properties of nearly silent flight.

Avians can be find everywhere in the world, in different sizes and colours. Even though wings gave birds the ability to fly, some bird species lost that ability (e.g. penguins, ratites, some endemic species). Various adaptations in their bodies can be seen, which effects the eating habbits or even the habitat [37, 44]. Some bird species have further evolved for swimming and some for fast flight. As said before, there are many different adaptations seen in birds.

By observing the nature, birds with a wingspan of 3.5 m (wandering albatross), or weights up to 17 kg (trumpeter swan) can be found. During the Pleistocene Epoch (approx. 2 million years ago) a bird called Teratornis incredibilis had an approximative wingspan of almost 5 m and was known as the greatest flying avian. On the other hand, the bee hummingbird with a size of 6.3 cm and weight of 3 gr is known as the smallest bird [19].

Overview of Birds with Low Noise Level Flight

Owls (Figure 1.1, left) are the first birds that came in to mind if low noise flight is the case. Since they are mostly nocturnal hunters they have to develope different features to take advantage over the prey. Therefore, the main ability of silent flight came forward. They hunt small mammals and other avians, although a few even hunts fish. The smallest owl weighing as little as 31g and measuring 13.5cm (elf owl) [33]. While the features that enables such flying abilities remain mainly unknown, the wing geometry and the feather anatomy are the primary research topics. These subjects will be explained in the further sections of this study.

Another bird – famous for its hunting skills – is the Falcon (Figure 1.1, middle). Falcons are medium sized birds of prey found all across the world and they are best known for their ruthlessness and their incredible flying abilities. Peregrine falcons have been recorded diving at speeds of 320 km/h, making them the fastest-moving creatures on Earth. The fastest recorded dive for one is 390 km/h [64].

In contrast to the other two species, Seagull (Figure 1.1, right) is a type of sea bird. There are over 20 species of seagulls that can be found all over the planet, the Little Gull with a weight and size of 120 g and 29 cm, and the Great Black-beaked Gull with 1.75 kg and 75 cm as the largest gull species. Seagull has strong body, elongated legs and webbed feet [14].

Figure 1.1: a) Owl – b) Falcon – c) Seagull.

While selecting these 3 types of birds, first, we paid attention to their size. They are very similar in size, so that their geometries are comparable. Another point is the hunting ground, which differs for all three of them, where we see distinct evolutions in terms of flight styles and anatomy. Since our study is based on the owl, we want to see "what makes the owl so silent flyer". Therefore, selecting birds with different flight behaviours and anatomy, gives us significant results for each bird.

1.2. Fundamentals of Birds

The wings of birds are adapted to operate over a wide range of flight styles, from the highly rigid geometries of gliding to the relatively flexible kinematics of flapping. These flight styles are extended further during take-off, landing and manoeuvring, while flying at high angles of attack and generating highly unsteady flows. All of this is obtained whilst operating in highly turbulent flow conditions.

To dive in further, the basics of planes are very alike with that of a bird flight, where the main actors of aerodynamic forces are drag and lift forces [68]. The wing is shaped such that an upward force is ensured on the wing by the flowing air, the so called lift force. The other dominant force, drag, is the reverse direction of flight motion, and because of that it is the reason of energy consumption flight [11]. Different from lift, drag can be divided into to two parts; lift-induced drag and parasitic drag. The lift-induced drag is the force, which is formed inherently as a result of lift generation, where parasitic drag is the combination of boundary friction and form drag [17].

As understood by the given information about the fundamentals of birds, it is obvious that both the anatomy and kinematic are related to the aerodynamics of avians. Therefore, the two topics (anatomy, kinematic) are reviewed seperately in the following sections.

Anatomy of Birds

Anatomically, a bird's wing consist of feathers that are attached to the movable skeleton. The wing feathering can be categorized as two main parts, flight (remiges) and covert feathers [77]. While hand-bones are bonded with primary remiges, secondaries are supported by the ulna (Figure 1.2). Anatomically and geometrically, the wing can be divided into proximal and distal part. The proximal part is exceptionally cambered and has a thick leading edge. Skeleton and muscles are related to this thickness. Therefore, several layers of coverts thicken this wing section. The trailing edge is very thin as only this part of the wing consists of single remiges. The wing area is build up just by overlapping primary feathers. Thence, the distal wing is extremely thin and low cambered [65].

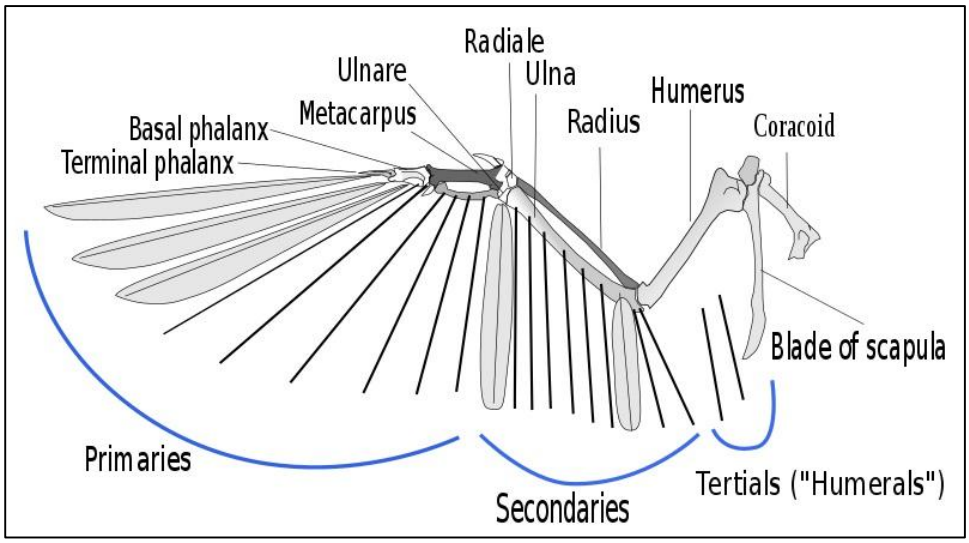

Figure 1.2: Anatomy of a bird's wing.

The large wing area of owl wings is achieved by large remiges that overlap with high ratio to strengthen the wing surface (Figure 1.3) [9, 65]. Even though owls are agile flyers [78], we have to bear in mind that owl wings are not only optimized for flight but also to reduce flight noise and protect the bird against cold, heat or wetness. As feathers determine the main parts of the body of owls, they are used as a camouflage to prevent being seen by prey or predators [73].

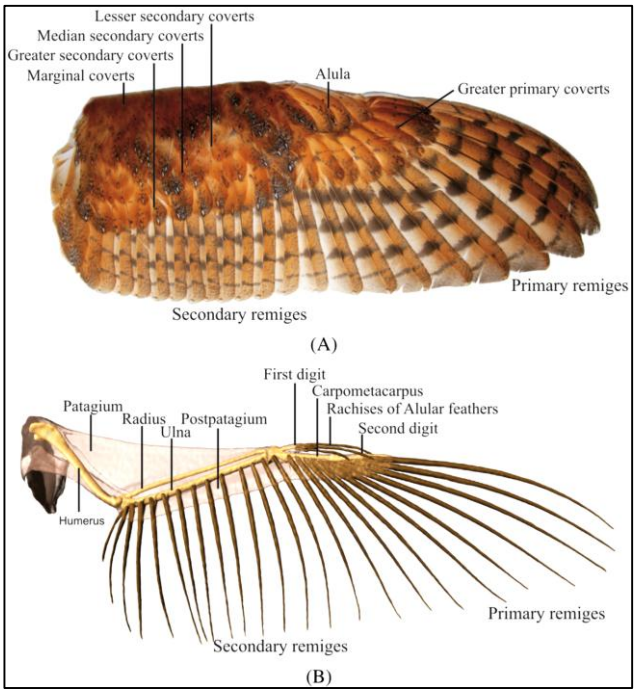

Figure 1.3: Barn Owl's wing.

Seagulls are between medium and large sized seabirds, with black patterns on the head and feathers [14]. The skeleton is formed of a shoulder, elbow and wrist. On the other hand, a short upper-arm bone provides a movement with the shoulder and wrist. A picture of a seagull wing is shown in Figure 1.4 [18].

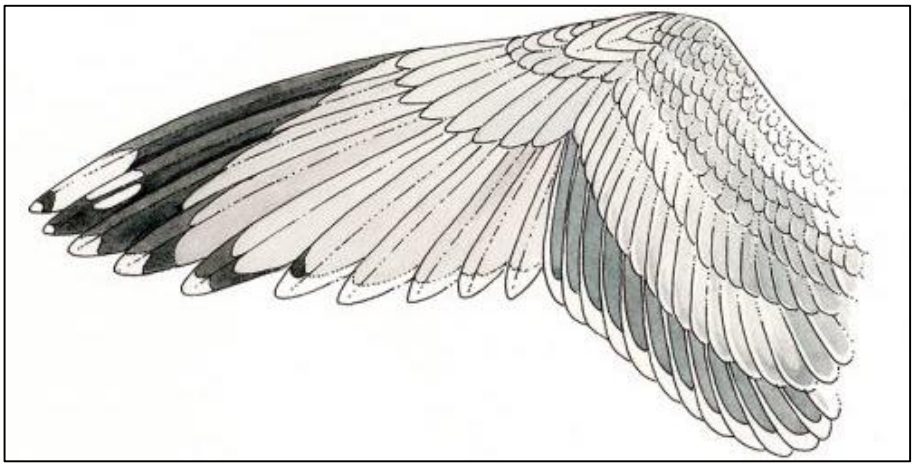

Figure 1.4: Seagull wing.

Falcons are specialized in highspeed flight (up to 320 km/h). To do this, the body must be very strong and relatively light in weight. Light enough to be able to take-off, but robust enough to carry the prey away (Figure 1.5). In some zones, there are supports in the bone structure to add some strength. Consequently, many bone volumes have sir cavities inside [15].

Figure 1.5: Falcon wing.

While owls using their hearing system to sense prey, they need to reduce flight noise. Flying slowly is one choice, but to provide enough lift at low-speed, the wing need to be highly cambered [58]. In comparison to other similar birds, owl wings show a special camber and thickness distribution, which provides enough lift at low flight speed [65]. More details about the aerodynamics of the wings will be examined further in this study in detail.

Kinematics of Bird Flight

This section sheds light to the flight styles of the birds. In this study, the flight is only investigated as gliding flight, whereas flapping flights is also common for every avian, but is not examined in this work. Wings produce lift, even without moving them, because the air flows faster on the top side than on the bottom side. This can be seen because of the cambered wing profile of birds, which allows the gliding flight. By moving the wings up and down (basically), lift will be generated by pressure reduction, which is called flapping flight [65, 49]. In combination with the anatomical properties, the birds can move their body, tail or wing in different angles. Therefore, the kinematics of avian flight are mostly the outcome of the anatomy [11].

Gliding Flight

For an optimal gliding flight, lift should be maximum, while drag is minimum. A good glider flies a long distances effortlessly, maintaining its altitude, but loses height with the effect of gravity [47]. Calculating the angle between avian motion and the horizon gives the gliding efficiency of a bird. The lift and drag forces influence this angle, through wing shape has also some effect on it [38].

Compared to narrow wings, wide wings can help a bird to soar longer at low flight speeds. Furthermore, to carry the prey up in the air, larger and wider wings provide additional lift. Therefore, especially falcons have longer and wider wings. [59].

While venturing out at sea, seagulls usually don’t have any places to take a rest. They must manage their energy consumption during flight, which is the reason for their advanced gliding abilities [25]. Seagulls developed their wing kinematics to take an advantage of the air current over sea during gliding. Since the air flow direction and magnitude is not constant, they morph their wingspan and adjust the camber degree of the wing to slightly glide on these air currents [2, 14]. By considering this, a detailed look at the structure of the upper-arm bone shows that the flight is easily setted with

the help of the wrist and shoulder [2]. The wing configuration alters with the rotation about the joints, as shown in Figure 1.6, and consolidated dihedral and sweep angles [18].

Figure 1.6: Wing adjustment of Seagulls a) one wing, b) both wings.

Taking a look at owls, relatively large, broad, rounded wings, with a large surface area relative to their weight, are seen. This low wing-load (body mass × 9.81 ms^{-2} / both wing areas) allows them to fly buoyant and easily, without much flapping. They can glide slightly and fly slowly for long periods of time, even at low flight speeds [46, 48]. Gamble et al. [36] studied the morphing effect of bird wings by using 3 types of airfoils (NACA 0012, a conventionally cambered and a reflex cambered) with 3 different sweep angles. The numerical solutions based on RANS turbulence model for low Reynolds number ($3{,}7x10^{4}$-$7{,}4x10^{4}$) flow. The results showed that morphing of sweep and camber gives a clearly advantage in terms of lift properties. Notably, in higher velocities, the sweep needs to be increased as much as possible.

Flapping Flight

Flapping flight takes place in two stages: the down-stroke and up-stroke. The first one is responsible for the major thrust, whereas the second one also ensure some thrust, depending on the bird type [52]. Avians use flapping flight for accelerating, but it is also important during take-off and landing. Most of the energy consumption occurs during these movements, which also increase the importance of the wing structure [66] Therefore, thickness as well as camber decrease towards the wing tip, so that a reduce in inertia is ensured, or the wing is lightly folded inwards at each up-stroke. Also avians throw their wings to the front before during down-stroke, so that it can push its body forward (Figure 1.7) [67]. This leads to wing beats at higher frequencies and much more energy efficiency [12].

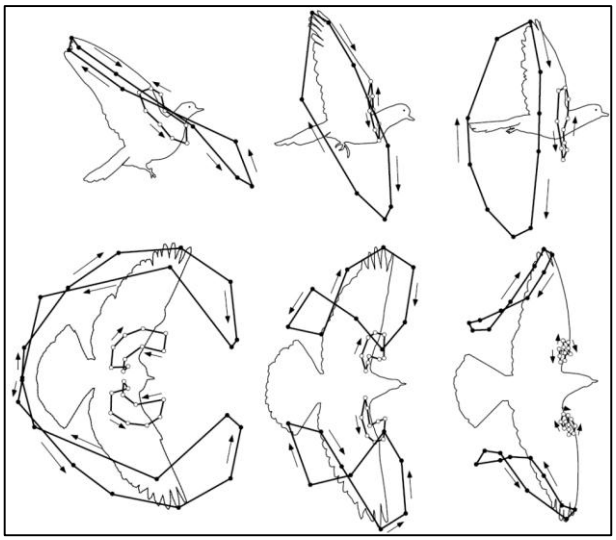

Figure 1.7: Wing motion of a pigeon.

Another adjustment is seen by setting up the angle of its wings it can fly faster or slower. As an example, when a falcon pulls its wings together close to its body (Figure 1.8), it reaches its highest flight speeds [59].

Figure 1.8: Wing shape of a Falcon during a fast flight.

The falcons pointed wings also help them to reach their renowned high flight speeds. The wings are pulled back and contributed to the bird's aerodynamic figure. The curved wings transform the whole body into an airfoil, which maximizes maneuverability, lift force, and flight speed [13, 75]. Mentioned in the previous sections, owls are capable of flying at small wing-beat frequencies and amplitudes due to the fact that they have large wing area and specific profile of the [9].

2. THEORETICAL BACKROUND, NUMERICAL SET-UP AND DESIGN

In this chapter, the theoretical backround and the setup of the numerical analysis which are carried out will be described, whereas a brief explanation about the design and meshing process will explained.

2.1. Aerodynamic – Sound Relation

It is known that a flow over a body can form a low pressure field at on side and high pressure field on the other side, except spheres or symmetric shapes. This pressure difference create a so-called lift and drag force [17]. Accordingly, lift and drag coefficients (C_l and C_d) can be mentioned at first place. The lift/drag coefficient is related to Reynolds number and the angle of the body to the flow (angle of attack). Thus, show that the main actors of flight; free-stream velocity, body dimensions and body to flow angle are included in the basic coefficients of aerodynamic. Therefore, these coefficient(s) gives a prescience about the aerodynamic characteristics of the investigated body, and since it refers to a 2D section, it can be correlated to the chord section and length [4].

In Figure 2.1, it can be understand that with increase in the angle of attack (AOA) the lift coefficient varries linearly till a maximum point. For the linear region of the graphic, it can be said that the flow is mostly attached to the body surface. Thenceforth, in the non-linear region the flow forms a wake (dead air region), where the flow starts to recirculating and seperates from the surface [4]. Knowing that, the maximum value of C_l determines the stalling velocity and is a very important for an airfoil performance.

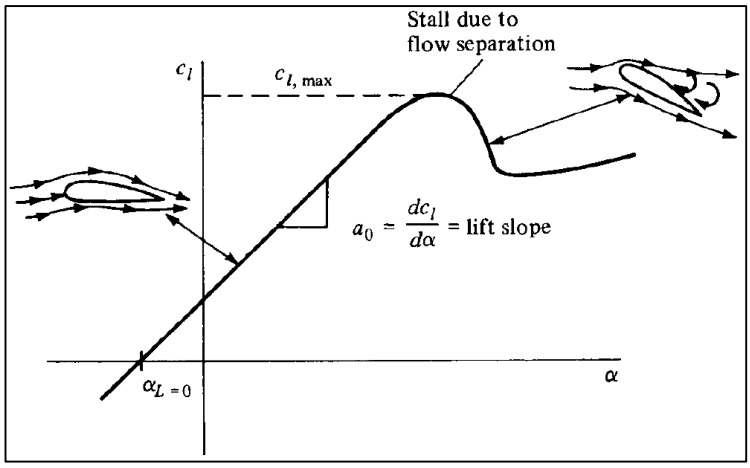

Figure 2.1: Coefficient variation with angle of attack for an airfoil.

For the low flight-velocities (low Reynolds numbers) of the owl (2.5-10m/s), flow separation will probably arises due to the pressure increase in the laminar flow regime. The changover to the turbulent flow at the separated boundary layer happens quickly, allowing a reattachment of the flow to the wing layer by the growth activities of the turbulent flow, which is shown in Figure 2.2 [4]. For all flying birds, airfoil's zones with low pressure occurs because of the difference in free-stream velocity throughout the wing shape. The highest reverse pressure gradient by an airfoil is limited, which can lead to flow separations by exceeding this. Consequently, this means that the flow starts to recirculating after this limit and seperates from the surface. [35].

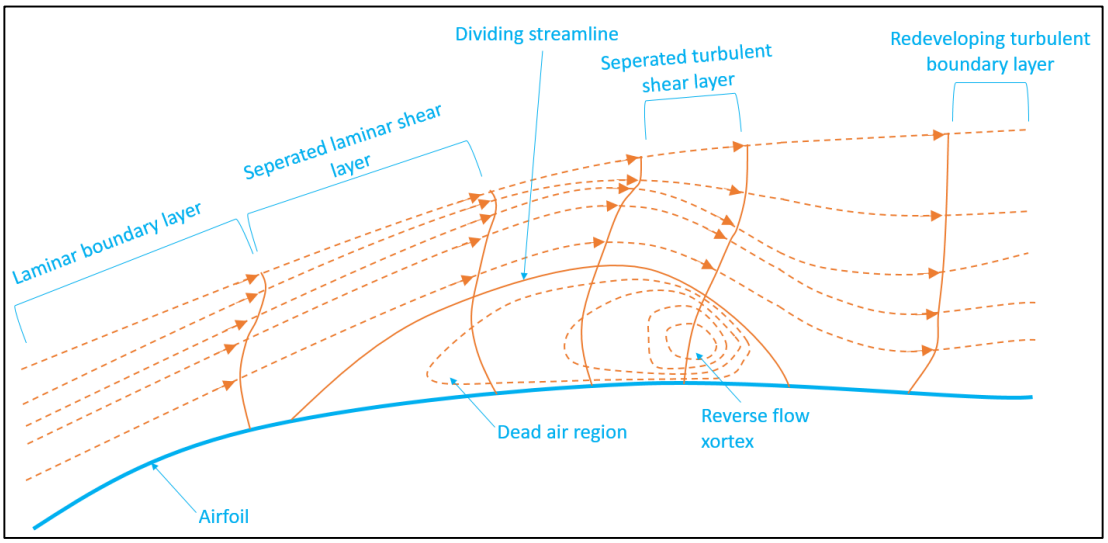

Figure 2.2: 2D Flow separation on an airfoil.

The vorticity proportion kept in the airfoil's boundary layers are related to the circulation of the 2D blade profile. Hence, asymmetrical airfoils, which are conceived for positive lift formation, shift the vorticity in the pressure side (figure 2.3) to the sucton side of the boundary layer. Therefore, the flow on the suction-side has a higher potential to seperate from the airfoil [4]. This condition can also be seen in the results of this study.

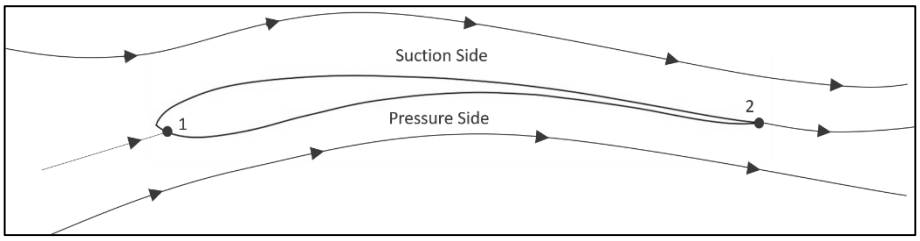

Figure 2.3: Suction and pressure side on an airfoil. 1 and 2 are stagnation points.

Since this study aims to analyse 2D airfoils basically, the Kutta condition can help to understand the vortex generation on an airfoil. The Kutta condition states that a flow around a body with a sharp corner creates a circulation, strong enough to keep the rear stagnation point at the trailing edge [1]. This phenomena can be seen in detail in figure 2.4 [35].

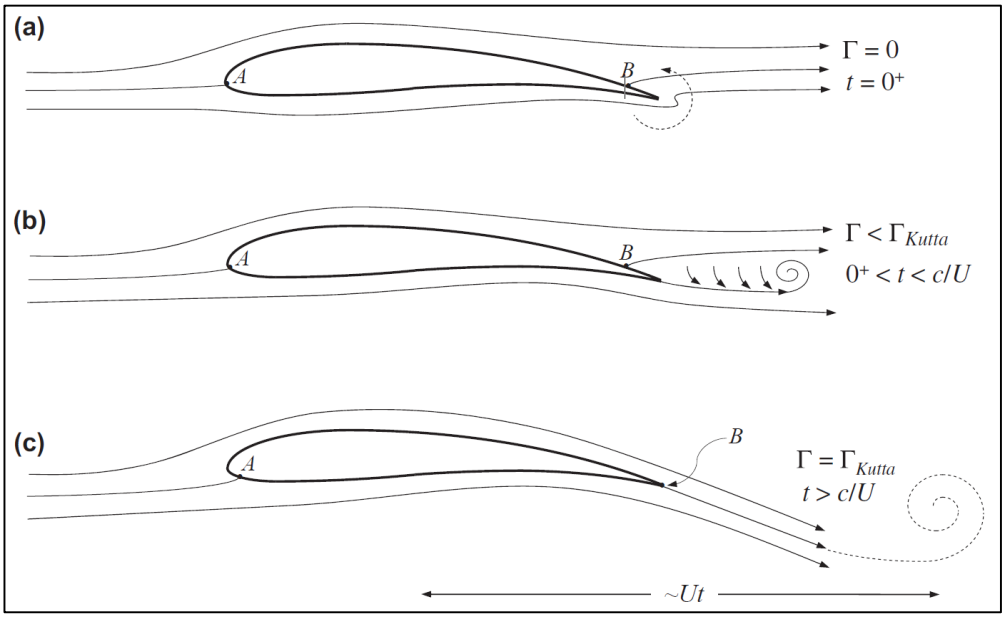

Figure 2.4: Flow types over a stationary wing profile at a low angle of attack under a horizontal flow.

Focusing on the trailing edge shape, the selected birds for this study have all different trailing edge shapes (see section 2.3.1). By taking a look at figure 2.5, the edge with the finite angle has two velocities with two different directions. This is physically not possible and the only explanation for this situation is that both velocities are equal to zero [35]. As a result of this, point a can be stated as the stagnation point. On the other side, the trailing edge with the cusp has two velocities in the same direction. By applying the Bernoulli's equation (1.1);

$$p_a + \frac{1}{2}\rho V_1^2 = p_a + \frac{1}{2}\rho V_2^2 \tag{1.1}$$

$$V_1 = V_2 \tag{1.2}$$

we can see that the velocities are finite and equal (1.2) in magnitude and direction [4]. Since the direction of the velocity is important for the flow that is leaving the airfoil, the trailing edge structure has a great effect on the vortex generation of bird wings and will be examined in the following sections in detail.

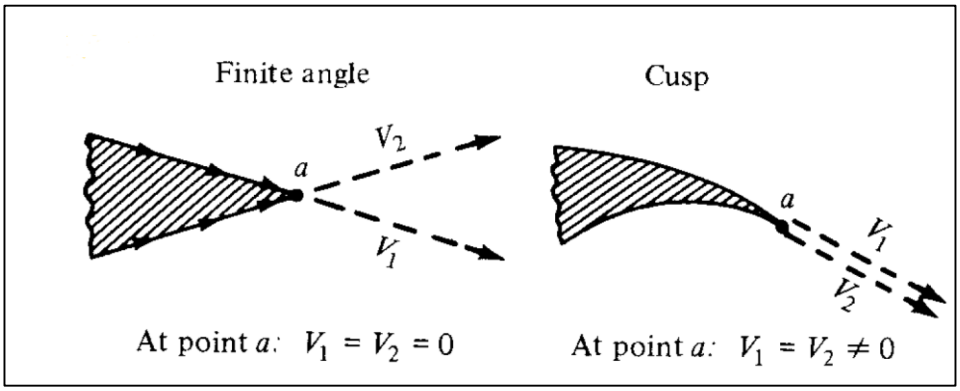

Figure 2.5: Kutta condition for different shapes of the trailing edge.

After explaining the fundamental effects of vorticity, velocity and pressure on airfoils, a brief entry into the connection to aeroacoustics can be made. Since, vorticity can be regarded as a basic phenomena for flows, it may also be an important actor for acoustics. Furthermore, the main variables to be investigated for aeroacoustic noise related to vorticity are velocity, pressure, density and temperature, where the last two are less relevant for our study [29]. All of these four variables can be defined with the wave equations. Conservation of mass describes the correlation between velocity and

density, where conservation of momentum represents the connection between velocity, density and pressure, and the thermodynamic equation of state relates the pressure, density and temperature [51].

$$\frac{\partial p'}{\partial t} + p_0 \vec{\nabla}.\vec{u} = 0 \tag{1.3}$$

$$p_0 \frac{\partial \vec{u}}{\partial t} + \vec{\nabla} p = 0 \tag{1.4}$$

$$p(\vec{x}, t) = B\left\{\frac{p'}{p_0}\right\} \tag{1.5}$$

Where B is the adiabatic bulk modulus.

Equation (1.3), (1.4) and (1.5) can then be added together into one equation, which depends on the fluctating pressure variable;

$$\nabla^2 p = \frac{p_0}{B}\frac{\partial^2 p}{\partial t^2} = \frac{1}{c^2}\frac{\partial^2 p}{\partial t^2} \tag{1.6}$$

where c is the speed of sound [51]. Equation (1.6) helps to understand the connection between the four main variables, which form vorticity.

After the velocity-pressure-vorticity relation is explained above, an introduction to aeroacoustics can be realized in a more understandable way. Starting with the monopole, dipole and quadrupole sources, which are directly related to the aeroacoustics, are very important to explain aerodynamically generated noise. Moving further with the definition of these sources, monopole (Figure 2.6) is a single, spherical sound source which radiates waves inward or outward. On the other hand, dipole (Figure 2.6) can be realized as two out of phase monopoles with same strength, where quadrupole is alike and consists of two out of phase dipoles [51].

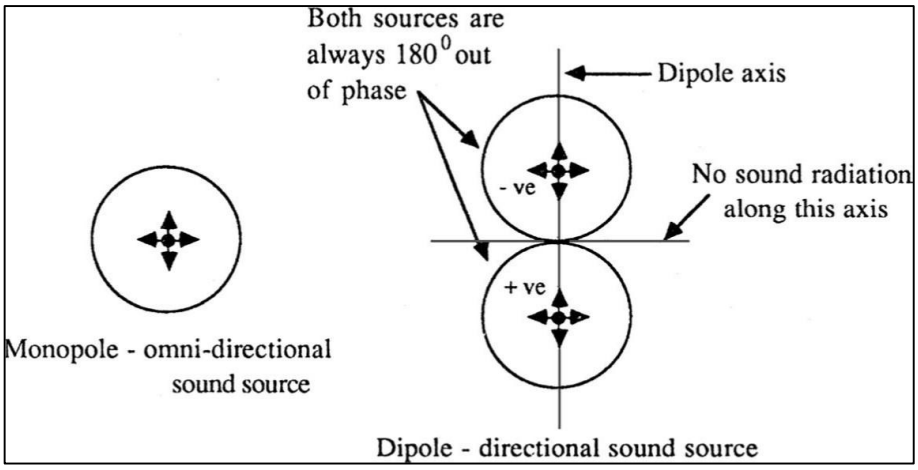

Figure 2.6: Monopole and dipole examples.

Note that the structures in figure 2.6 shares similarities with vortices. Both have a direction, a strength and are based on velocity. While monopoles interact with each other and form new type of sources (dipole, quadrupole), the same situation occurs also in vortices, which can form complex structures by affecting one another. In figure 2.7, the streamlines of a dipole source and two vortices is illustrated to realize the similarities between them [54].

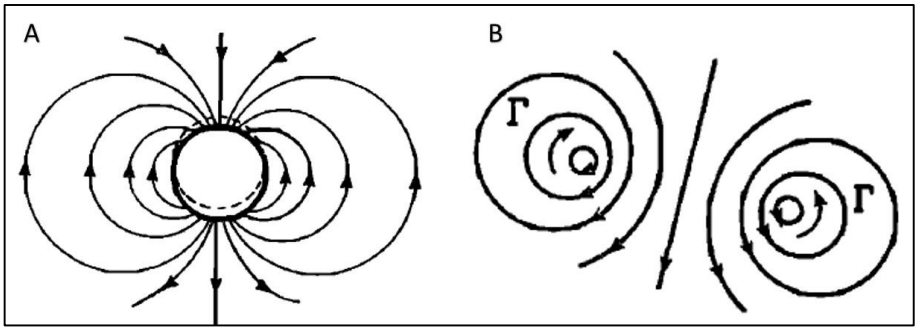

Figure 2.7: Streamlines of A) dipole source and B) vortices.

Furthermore, the sound power radiated of these sources in terms of velocity potential are given in the equations below:

$$\Pi = 4\pi r^2 I(r) = \frac{Q_{rms}^2 k^2 p_0 c}{4\pi(1 + k^2 a^2)} \tag{1.7}$$

By implementing $Q = L^2 U$ and $k = U/L$ to equation (1.7);

$$\Pi \approx \frac{L^4 U^2 p_0 c U^2}{4\pi L^2 c^2} \approx \frac{L^2 U^4 p_0}{4\pi c} \tag{1.8}$$

Also for dipole;

$$\Pi = \frac{Q^2 k^4 d^2 p_0 c}{3\pi} \tag{1.9}$$

By implementing $Q = (2d)^2 U$ and $k = U/2d$ to eqation (1.9);

$$\Pi \approx \frac{(2d)^4 U^2 U^4 d^2 p_0 c}{(2d)^4 3\pi c^4} \approx \frac{p_0 d^2 U^6}{3\pi c^3} \tag{1.10}$$

On the other hand for quadrupole;

$$\Pi = \frac{4Q_{rms}^2 p_0 c d^4 k^6}{15\pi} \tag{1.11}$$

By implementing $Q=(2d)^2U$ and $k=U/2d$ to equation (1.11);

$$\Pi = \frac{4Q_{rms}^2 p_0 c d^4 w^6}{15\pi c^6} \approx \frac{p_0 d^2 U^2}{15\pi c^5} \tag{1.12}$$

By implementing $k = 2\pi/\lambda$ to (1.8), (1.10) and 1.12), where λ is the wavelength, and comparing the equations below,

$$\frac{\Pi_D}{\Pi_M} = \frac{4k^2 d^2}{3} \sim \left\{\frac{d}{\lambda}\right\}^2 \tag{1.13}$$

$$\frac{\Pi_Q}{\Pi_M} \sim d^4 k^4 \sim \left\{\frac{d}{\lambda}\right\}^4 \tag{1.14}$$

it can be seen that the monopole sources are the most dominant one in terms of sound power compared to the other two source types at low frequencies (long wavelengths). On the other side, at high frequencies the situation is vice a versa [51]. This outcome will be also helpful in explaining the acoustic results further in this study. Considering these equations, it is seen that monopoles are proportional to the fourth power of the flow velocity, where dipoles are to the sixth power and quadrupoles (both lateral and longitudinal) are proportional to the eighth power of the flow velocity [29]. This is

important since the flow velocities change in the analysis of this study, and it will help to understand the noise variety in the different cases.

2.1.1. Bird Flights Researches

As we know now, bird species varries in many different aspects. Each feature is adapted to the environment, which is the bird living in. Since our topic is the flight behaviour of them, especially the flight noise levels, we will only introduce the researches related to aeroacoustics. Most of the studies are based on specific parts of the birds, which are directly connected to acoustic characteristics.

First, Mascha [45] mentioned the serrations on owl wings and identified the outstretched pennula as a source of the mild wing layer of owls, also known as velvet-like surface. Hertel [27] derived an explanation of how the velvet-like upper surface may prevent generated sound. He claimed that it act as a kind of cushion so that it reduce the noise during flight. In another study by Schwind & Allen [61] the flow over an airfoil with and without serrated trailing-edges were investigated. Measurements at low Reynolds numbers ($2.5x10^4$) show that, barbules most effectively dissipated the leading-edge separation bubble by generating vortices on the airfoil's upper surface. Further, the serrations reduced the peak values in average pressure for high Reynolds numbers ($1.2–6.2x10^6$) up to 41%. Bachmann et al. [8, 9], investigated the velvet-like wing structure and how the flow distribution over the wing surface affects the noise generation potential. A certain pattern distributes the turbulence into smaller vortices called micro-turbulences (Figure 2.8). After that the fringes at the edge absorb the generated noise of air flowing over the wing and changes the directon of air flow.

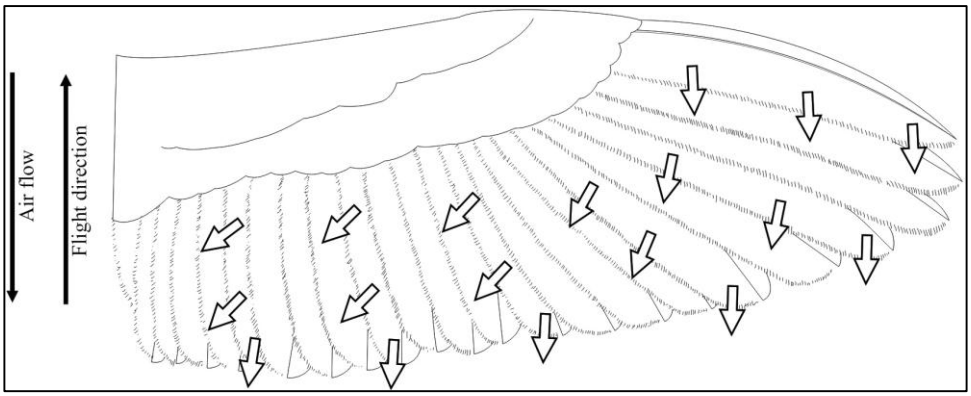

Figure 2.8: Effect of velvet-like structure of Owl feathers on air flow. Serrations are breaking large turbulences down into small.

Neuhaus et al. [50] examined a tawny owl (Strix aluco). The recorded noise during flight reaches its most intense range between 200 and 1500 Hz. In flapping flight, the emitted sound did not change after removing the serrations on the leading-edge. Only a increase before landing was seen. Furthermore, wind tunnel experiments show that the flow over the owl wing have a more laminar flow character compared to the flow over wings of other bird species. Another scope was made to the leading-edge by adding serrations again, but with different numbers of teeth. Ito [30] investigated its profiles with two Reynolds numbers ($2.1x10^4$ and $2.1x10^5$) to show the behaviour of the flow in low and high speeds. By increasing the number of teeth, it is seen that the flow improves its aerodynamic properties in low Reynolds number region, in turn, no significant changes are seen for high Reynolds number region.

Not only the leading-edge, also the trailing-edge is an important feature for silent bird flight as mentioned in previous sections. Weiyang et al. compared an SD2030 airfoil with and without serrated trailing-edge in a wind tunnel experiment [74]. Microphones were placed near the trailing to record noise and also near-filed turbulence measurements were conducted. The velocities for the experiment were 21 m/s, 25 m/s and 31 m/s and the AOA was set to 0°. The results show that serrations clearly reduce the noise (average of 5dB), but affects the turbulence at different points. On the other hand, Liang et al. investigated the same airfoil with Large-Eddy-Simulation and Ffowcs-Willams & Hawkings analogy [40]. An overall 3.3dB reduction in noise was seen with the serrated trailing-edge, wherease, the main source of noise generation was the shedding of seperated vortices.

When talking about acoustics, a theoretical noise production model developed by Lilley [42] showed that the sound is mainly created by the trailing edge of the wing for aircrafts and birds. In case of an owl, the velvet-like wing surface, trailing-edge feathers and body and legs combined reduces the generated noise, especially in the frequencies above 2 kHz.

To continue with numerical studies, Agrawal and Sharma [3] analyzed the serrations in owl plumage at the leading edge, which were numerically modeled, to study their impact on reducing in turbulence noise. Large eddy simulation methodology was used with Ffowcs-Willams & Hawkings analogy. The selected profile was a NACA 0012, where the chord related Reynolds number was Re = 4.8×10^5. A cylinder was placed in front of the airfoil to generate unsteady pressure distribution. Results show that the Power Spectral Density (PSD) of measured and predicted data match at the peak frequency. In general, a noise reduction of up to 5dB was seen.

Turning to experimental works, Chen et al. [16] investigated the sound absorption mechanism of the owl by Stereo Microscope (SM), Scanning Electron Microscopy (SEM) and Laser Scanning Confocal Microscope (LSCM). Comparisons between the owl and buzzard were carried out for flight measurements in an anechoic chamber, whereas the sound absorption measurements for the wing feathers are taken place in an impedance tube. The results show that the owl feathers has better noise suppression properties than the buzzard feathers (at 6 kHz 0.13 for owl, 0.08 for buzzard). Additionally, the sound pressure level for the flight experiment at every measured frequency was lower for the owl (at 6 kHz 18dB for owl, 26dB for buzzard).

Geyer et al. [23] performed indoor and outdoor measurements to demonstrate difference between the noise levels of the owl compared to the noise of non-silently flying birds. The outdoor experiment was carried out with owl, flying over a microphone array. The indoor measurements were performed with prepared wings of owl, hawk and kestrel at fifteen flight speeds between 5 m/s and 20 m/s at 0°, 8° and 16° AOA. Measurements took palce between 500 Hz and 10 kHz. Results of both experiments show that the owls generate less noise than the other birds used in the studies. No major noise difference was measured at low frequency level, but for mid and high frequency range, the owl outperformed the other birds in case of silence.

2.2. Computational Details

2.2.1. Turbulence Model

In fluid dynamics, fluid motion described by irregular variations in pressure and velocity are called turbulence. Turbulence is formed by overbundant kinetic energy in regions of a fluid flow, where the the fluid's viscosity damping effect bypassed [10]. In general terms, interacting unsteady vortices appear of many sizes can be seen in turbulent flows (figure 2.9) [35].

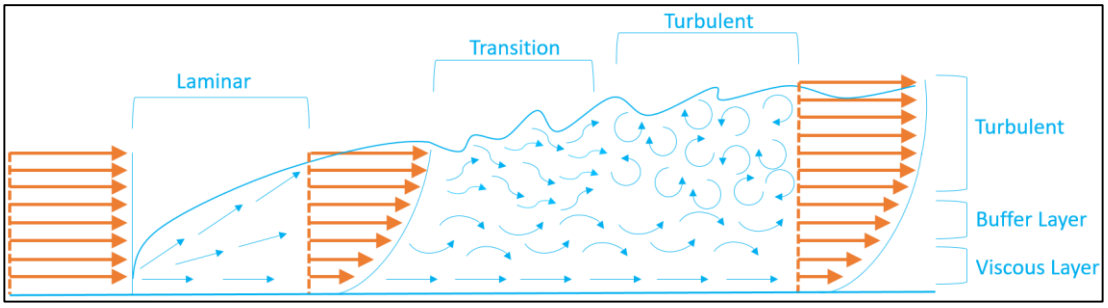

Figure 2.9: Turbulence generation over a flate plate.

For simple cases of turbulent flow, equations can be solved directly, whereas complex turbulent flows, CFD simulations predict the outcome of turbulence. These simplified turbulence models are equations that predict the statistical formation of turbulent flows [53].

In order to choose the right turbulence model, the case which is going to be solved must be defined properly. Since every model has its own characteristic features for different cases, it is very important to determine a suitable model. Therefore, the most common models will be investigated in this section.

Starting with Spalart-Allmaras, a low Reynolds number model, which is developed for aerodynamic applications. Studies shows that this model has some weakness in computing shear flow, separated flow, or decaying turbulence, but it’s advantageous in terms of convergence and stability. For example X. Liu and X. Liu [43] used this model in the steady flow over an owl-wing based airfoil for pressure and velocity coupling. Since, the Spalart-Allmaras model has been shown to realize decent results for applications involving wall-restricted flows and boundary layers subjected

to reverse pressure gradients, it was used for our steady cases and as the RANS model (combined with Detached-Eddy-Simulation) in our transient cases.

Secondary, the k-ω SST model is a very common turbulence model, which combines the k-ω and the k-ε models to a more compact approach. It is a low Reynolds number model, just like Spalart-Allmaras, with better free stream and near wall resolutions, which makes this model more exact and reliable for diverse class of flows. S. Hosder et al. used this model and come to conclusion that it gives better overall accuracy in different types of flows compared to k-ω and the k-ε turbulence models [28]. Because of the damped cross-diffusion derivative term in this model, some problems occur in the near-wall vorticity resolution for our case. Therefore, it was not appropriate for the analysis in this study.

Large eddy simulation (LES) is a transient technique in which the large eddies are resolved directly, while small eddies are modeled. That is because large eddies are more problem subjected, whereas, small eddies are less dependent on the geometry and tend to be more isotropic. In comparison to RANS models, LES is able to predict the vortex shedding and flow recirculation accurately. In contrast, LES has to be run for a sufficiently long flow-time to obtain a stable solution and can only be applied to 3D models. Thus lead to computational costs, which are higher than that of the steady RANS calculations. In a study, C. Rao et al. choose the LES turbulence model to investigate a flow over a single feather of an owl, because of its capability of resolving laminar-turbulent transition [55].

Adding together these information, RANS and LES has its own pros and cons. Thus lead us to another model for our study, the Detached-Eddy-Simulation (DES), which is a hybrid LES-RANS model. This model use the RANS for the wall limited flows, whereas the LES for the far-field. The DES model requires more computational costs than RANS, but requires less than LES. It also has 3 different options for the RANS selection, Spalart-Allmaras, k-ω SST and k-ε [5].

In this thesis, the Spalart-Allmaras was selected for the steady analysis, because it has been shown to give good results for applications involving wall dependent flows. The DES, with Spalart-Allmaras as a submodel, was chosen for the transient cases, while the LES was only available for 3D analysis, and it capabilities of solving the wall bounded and far-field flows was better than RANS models. The submodel decision was made so that the analysis all have the same RANS model. In general,

better vortex shedding and turbulence resolution was obtained compared to RANS, whereas computational costs were much less than LES.

2.2.2. Acoustic Model

After the relation between sound sources and vorticity is explained in section 1.4., a smooth transition to the acoustic models can be made. There are different approaches in terms of acoustic. Starting with the first one, the Lighthill's acoustic analogy. Lighthill generated a wave equation by using the Navier-Stokes and continuity equations. The equation below shows the analogy developed by Lighthill:

$$\frac{\partial^2 p'}{\partial t^2} - a_\infty^2 \Delta p' = \boldsymbol{\nabla}.\boldsymbol{\nabla}.\underbrace{(p\boldsymbol{vv} + (p' - a_\infty^2 p')\boldsymbol{I} - \boldsymbol{\tau}}_{\boldsymbol{T}} \tag{2.1}$$

The quantity T is called Lighthill's stress tensor, which contains variations in stream velocities (ρυυ), in entropy (ρ´- a^2_∞ ρ´) and in the viscous friction stresses (τ). This approach not only consists of the generated noise, also includes the flow convection and the gradual dissipations by conduction and viscosity. This is an advantage of this analogy, where every method of conventional acoustics is applicable and the solution of the aero-acoustic problem is basic. Unfortunately, Lighthill's analogy cannot describe kinematic effects, because refraction at shear- or boundary layers appear as sources. Several generalized wave equations have been derived after Lighthill, in the attempt to isolate those drawbacks, which could be stated as true sources of sound [41].

ANSYS Fluent offers one acoustic source equation, the Ffowcs-Williams & Hawkings (FW-H) wave equation. In general, it takes the Lighthill's equation as base, where a control surface is used to retain the monopole and dipole sources. Despite that, the effect of quadrupole sources, which are outside of the control surface, can be added with the Lighthill Tensor [76].

$$\begin{aligned} 4\pi a_\infty^2 H p'(x,t) \; = \nabla_x \cdot \nabla_x \cdot \int_{V_B^+} \frac{\boldsymbol{T}}{r|1-M_r|} dV(\eta) \; - \\ \nabla_x \cdot \int_{\partial V_B} \frac{(-\boldsymbol{\tau} + p'\boldsymbol{I})\boldsymbol{n}}{r|1-M_r|} dS(\eta) + \frac{\partial}{\partial t} \int_{\partial V_B} \frac{p_\infty v_n}{r|1-M_r|} dS(\eta) \end{aligned} \tag{2.2}$$

The first term of equation (2.2) is the unsteady flow volume, a quadrupole noise, which correspons to the sound generating turbulent eddy. The loading noise is the next term, while the last one is known as thickness noise. The second term can be connected with the aerodynamic force on the body surface. Not to forget that the thickness noise for non-moving objects drops [76].

Mentioned in the previous sections, the described equations can be used only with transient analysis in ANSYS Fluent. The acoustic results, which are related to the Ffowcs-Williams & Hawkings (FW-H), will be presented in the upcoming chapters.

2.3. 2D Design, Mesh and Setup

2.3.1. 2D Design

It is hard to define a standart 2D profile for avian wings, since they are vary from bird to bird, from species to species. Many different methods are used to find a similar profile for specified birds. In some studies you can find pairing approaches in which each bird wing associated to the most alike standart airfoil profile [70]. Others tried to scan a real wing and reproduce it in computational environment. A 3D noncontact laser scanner, [65] Projected pattern correlation technique [78] or a clinical tomography scanner are some of these kind of methods [7].

As said above, different techniques are used for creating an avian wing profile. But, for this study, the owl (Figure 2.10a) and gull (Figure 2.10b) profile given by Liu et al. [65] and the falcon (Figure 2.10c) profile given by V.A. Tucker and G.C. Parrott [70] are used as 2D airfoil profile for the following CFD analysis. The owl profile is extracted from the cross-section at the 40% of the wingspan, where the falcon and gull have standart profiles, RAF19 and S1223 respectively.

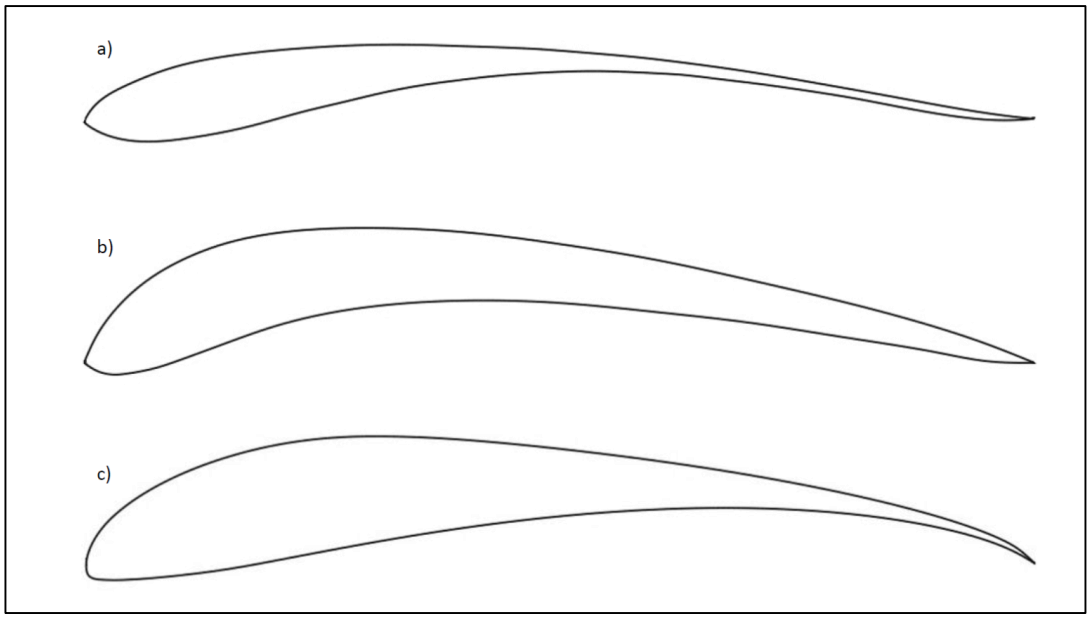

Figure 2.10: 2D profiles of a) owl, b) falcon, c) gull.

Considering the chord length for these birds, all airfoils are normalized according to the owl wing, because our main scope is the silent flight of the owl. To show the difference between the chord lengths, some measured examples are given in table 1 [6, 22, 26, 69, 70]. Furthermore, we tried to find a common point, which is 0.150 m and is based on an owl wing [6, 22, 40].

Table 2.1: Different chord lengths of owl, falcon and gull.

Bird	Min. Chord Length (m)	Max. Chord Length (m)
Owl	0.100	0.180
Falcon	0.195	0.220
Gull	0.085	0.110

As seen in Figure 2.10, differences between each airfoil is clearly visible. The thickness of the owl is far thinner (after 40% of the chord, thickness is ~3% of chord length) compared the other two profiles, whereas, the falcon has a relatively constant thickness throughout the camber line [7]. On the other hand, the gull profile thins down (at 70% of the chord) towards the trailing edge. This is also the case for the owl, which is a peculiar feature for it. Another remarkable property, for all three of them, is the trailing edge. The owl has a slope upwards, whereas the falcon has a tangential edge to its profile, at least the gull has a slope downwards. Here we can clearly see that

avians have unique wing structures. Knowing from the previous sections, the most important reason for noise generation was stated as the structure of the second half of the chord length (trailing edge part).

2.3.2. Mesh

The domain and the mesh of the airfoils are shown in Figure 2.11 and Figure 2.12, respectively. The distance from the airfoils leading edge to the upstream and downstream is 20c and 40c respectively. The minimum grid size on the airfoil edge is 10^{-3}, while the average skewness is 0,13 and the average orthogonal quality is 0,97. Due to limited computational resources the mesh size is set between coarse and medium quality.

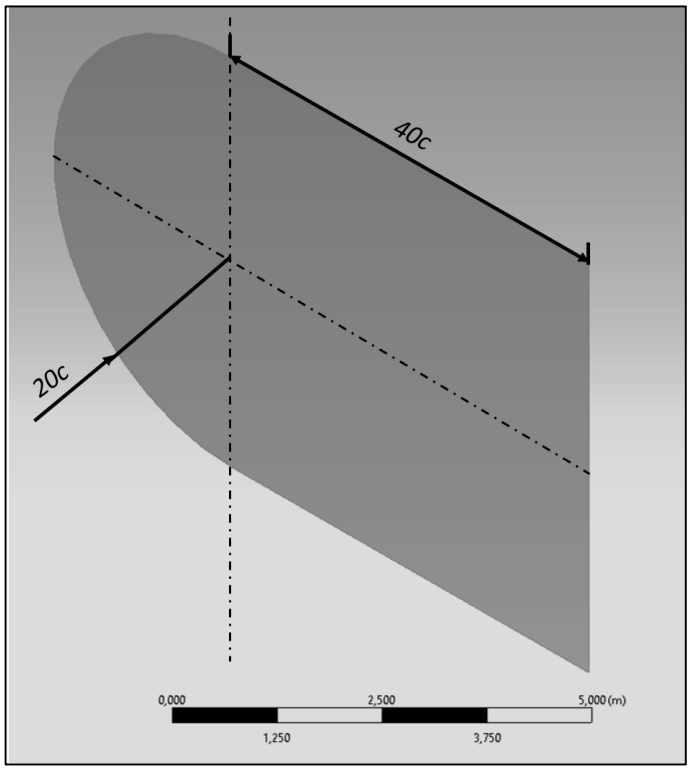

Figure 2.11: Domain of airfoils.

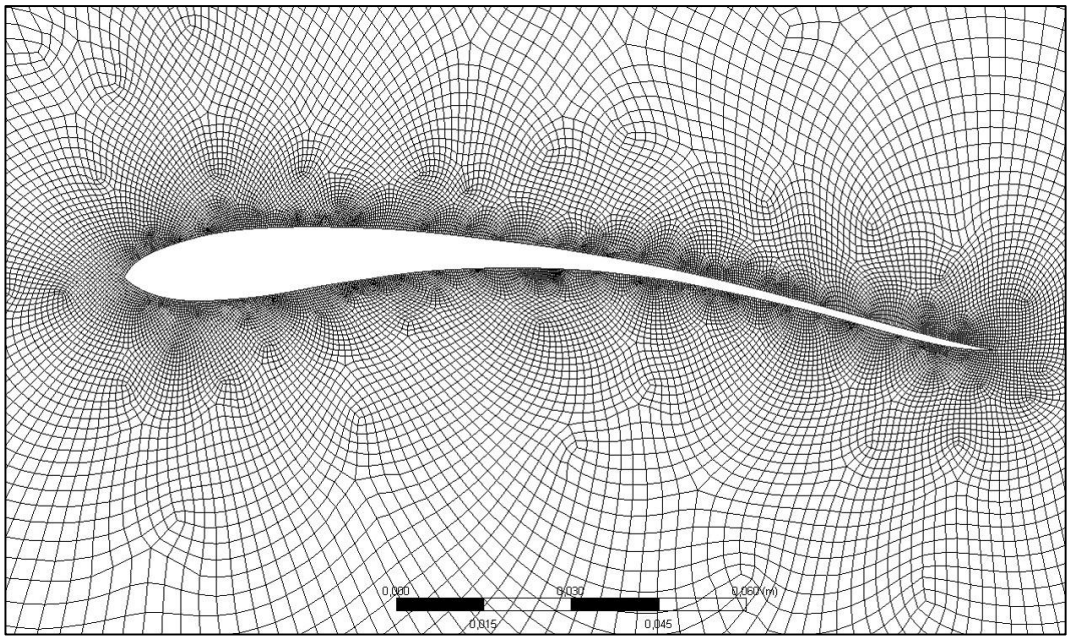

Figure 2.12: Mesh detail of airfoils.

2.3.3. Setup

Same as defining the normalized chord length, adjusting the velocity and AOA is another critical point for this study. Falcon is flying at high speeds (see section 1.2), while owls and gulls are flying at relatively lower speeds. Again, the owl was choosen as base bird for velocity and AOA. So, we can see the situation that will occur when the owl has the wing features of the other two birds. According to Neuhaus et al. [50] the highest flight speed of the owl is only about 6 to 10 m/s, where Mebs and Scherziger [46] stated that speeds in the range of 2.5 m/s to 7 m/s are valid for owls. Considering this, the maximum and minimum velocities are choosen as 2,5 m/s and 10 m/s. Additionally, 5 m/s is also selected to represent the transition speed between the two end speeds. Chord based Reynolds numbers are 2.6×10^4, 5.2×10^4 and 10.5×10^4. There are also wide range of options for AOA, but 0°, 5° and 10° were chosen according to gliding flight angles [22, 31, 32, 43].

Comming to the numerical setup for the transient anlaysis, DES model is used as turbulence model, which was mentioned before in detail. The Courant–Friedrichs–Lewy (CFL) number is a condition for the stability of unstable numerical methods. The CFL number should be close to 1, or even smaller. Therefore, it is adjusted to C=10, C=5, C=2.5 according to free stream velocities of 10 m/s, 5 m/s and 2.5 m/s

respectively. In the equation (2.3), a is the velocity magnitude, Δt is the timestep and Δx is the length between mesh elements.

$$C = a\frac{\Delta t}{\Delta x} \tag{2.3}$$

Since Δx, a and C is already defined, the timestep (Δt) is 10^{-3}s as a matter of course. This timestep is used for the transient analysis, and to ensure an analysis for 2 seconds, the number of time steps is set to 2000.

The numerical setup for the acoustic analysis depends on the Nyquist–Shannon sampling theorem. When a function f(x) without frequencies higher than Z hertz, it is defined by giving its ordinates at a series of points spaced 1/(2Z) seconds apart [62]. Stated by Sarradj et al. [60], at frequencies higher than 6.3 kHz the owl generated noise couldn't be measured with microphones. Therefore, a max frequency of 7.5 kHz is considered as sufficient for the acoustic analysis, which corresponds to a sampling frequency of 15 kHz. By applying the Nyquist–Shannon sampling theorem a timestep value of $\Delta t=6.6\times10^{-5}$ is required, while the timestep number of 1.5×10^{4} ensures a flow time of 1 second.

Moreover, receivers need to be defined for the FW-H acoustic model. Considering this, it is seen that in wind tunnel measurements the receiver positions are between 0.6-1 m, every angle of 24° around the wing specimens [23, 34]. At the same time, experiments carried out with prepared airfoils have the same pattern for the microphone distance [21, 72]. However, chord length based parameters are used in numerical studies e.g. 15x chord or 18x chord with 30° spacing [39, 43]. In this study, the receiver placement is accomplished within a radius of 1.5 m, which corresponds to 10 times the chord length, with angular difference of 20˚ between the receivers. A total number of 18 receivers are placed around the 2D airfoil.

3. RESULTS

This chapter is based on the two-dimensional numerical analysis of owl, falcon and gull wing cross-sections. The basic characteristics such as pressure, velocity and vorticity are used for comparison, and the analysis of the two-dimensional properties of the wing profiles are discussed. Nine cases for each airfoil are investigated, where three different free-stream velocities with three AOAs are combined as an analysis matrix. The following analysis are carried out as steady state and transient cases.

3.1. Steady State Results

3.1.1. Pressure Distributions

Looking from a general perspective to figure 3.1, it can be seen that by increasing the AOA in all three velocities, negative pressure areas on the pressure side decreases for owl wing. Especially for the free-stream velocity of 2.5 m/s the size of the negative pressure at the pressure-side is approximately 20% of the chord for 0°, 10% for 5° and 0 for 10°. This can be considered as a result of the special camber of the owl.

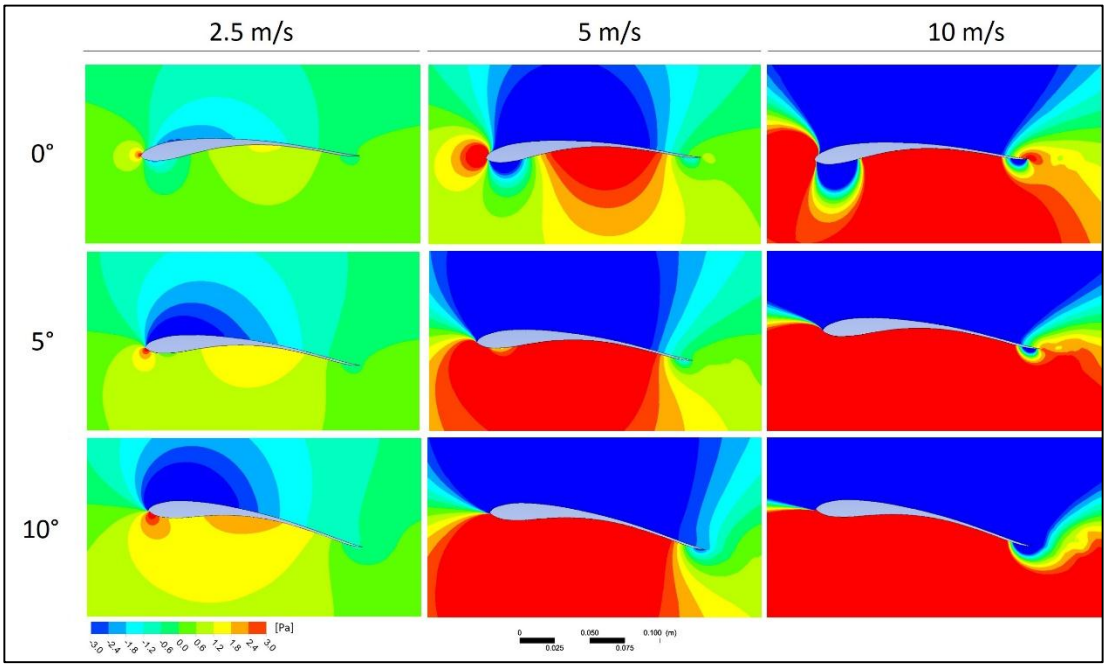

Figure 3.1: Absolute pressure contours for owl airfoil.

Similarities in the camber structure is noticed in figure 3.2 for the falcon and owl airfoil, where the lower side of both profiles have a curve with a (mostly) constant radius. Therefore, negative pressure at the pressure side can be seen at 0° AOA for all velocities, same like in figure 3.1. Different from the owl, the negative pressure contours almost disappear at the pressure side for 5° AOA, which is an outcome of the shape difference between the airfoils. The thickness after the half chord length is much larger for the falcon that leads to a more flat airfoil profile than the owl.

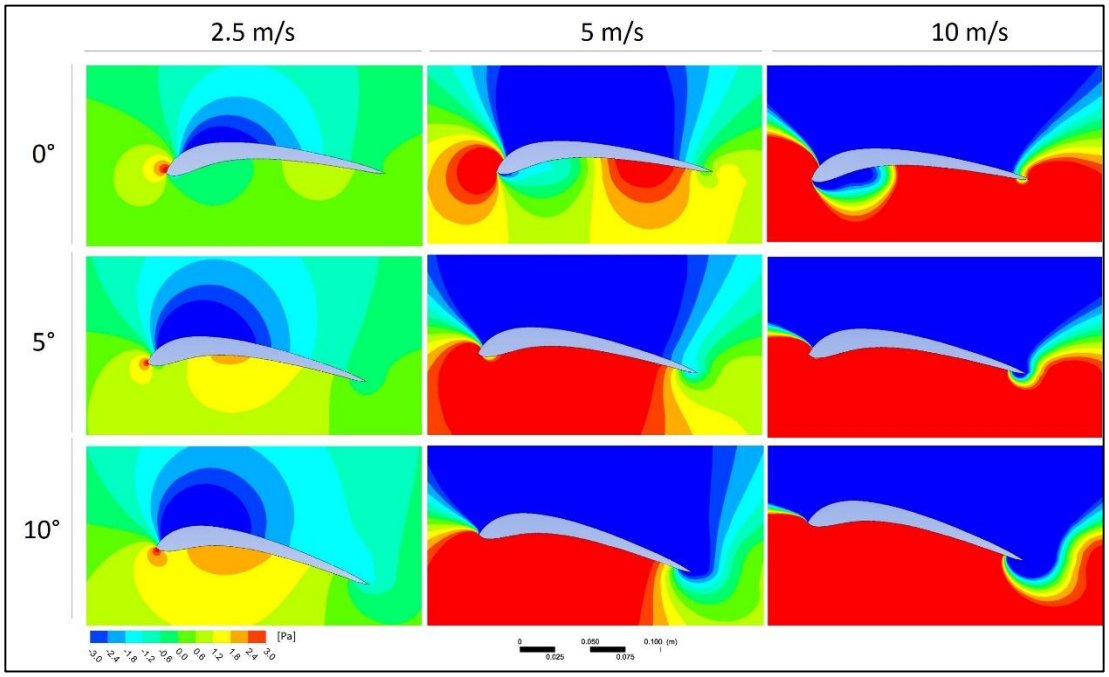

Figure 3.2: Absolute pressure contours for falcon airfoil.

The smallest area of the minimum negative pressure on the pressure side is seen in the gull airfoil (figure 3.3), since it has a flatwise geometry on the lower side of the firts half of the chord compared to the other two airfoils. Further, the trailing edge is distinct for the three airfoils (figure 1.13, figure 2.2), which has a direct effect on the flow leaving the airfoil. Taking the 10 m/s column as reference, the negative pressure area is the smallest for the falcon at 0°. By increasing the AOA to 5°, the negative pressure size increases for all of them, where the owl and the falcon contour sizes are similar to each other (approx. 10% of the chord length), and the gull has the largest of them (approx. 15% of the chord length). At 10° AOA, the negative pressure zones at the trailing edge reach their maximum, and the sizes are 20% for the owl, 25% for the falcon and 28% for the gull. Here, the effect of the trailing edge shape is seen clearly.

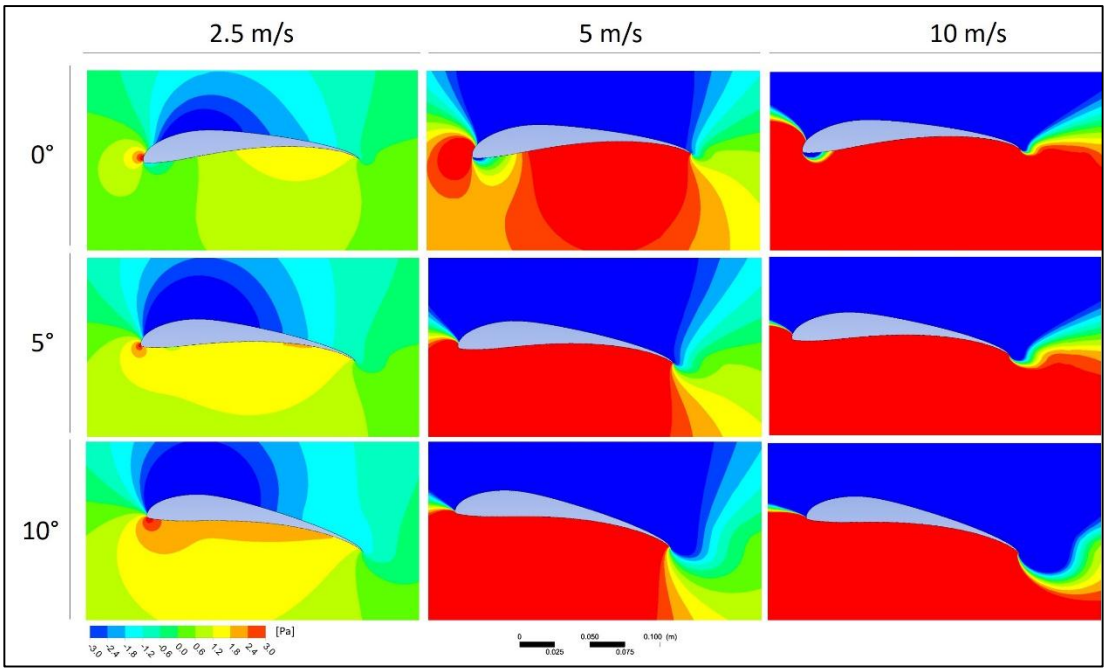

Figure 3.3: Absolute pressure contours for gull airfoil.

3.1.2. Velocity Distributions

The velocity results the leading edge zones show some similarities with the pressure contours for the three birds. However, the flow contours after 10% of the chord has some distinctive profiles to examine.

In figure 3.4, it is noted that the minimum and maximum velocity contours are varying with both velocity and AOA values. Regarding the 0°-2.5 m/s results, the min velocity (0-1 m/s) on the pressure side starts at 15% of the chord, and reaches till 65% of the chord. This type of contour is only available in 0°-2.5 m/s conditions. But the 10° AOA results have examples for 0-1 m/s contours on the suction side, where the starting point of this contour is located at 80% of the chord for 2.5 m/s and for 5 m/s at 86% from the leading edge. In general, it can be said that the velocity contours on the suction side mostly stays in the mid range of the scale for the owl, which is a remarkable feature.

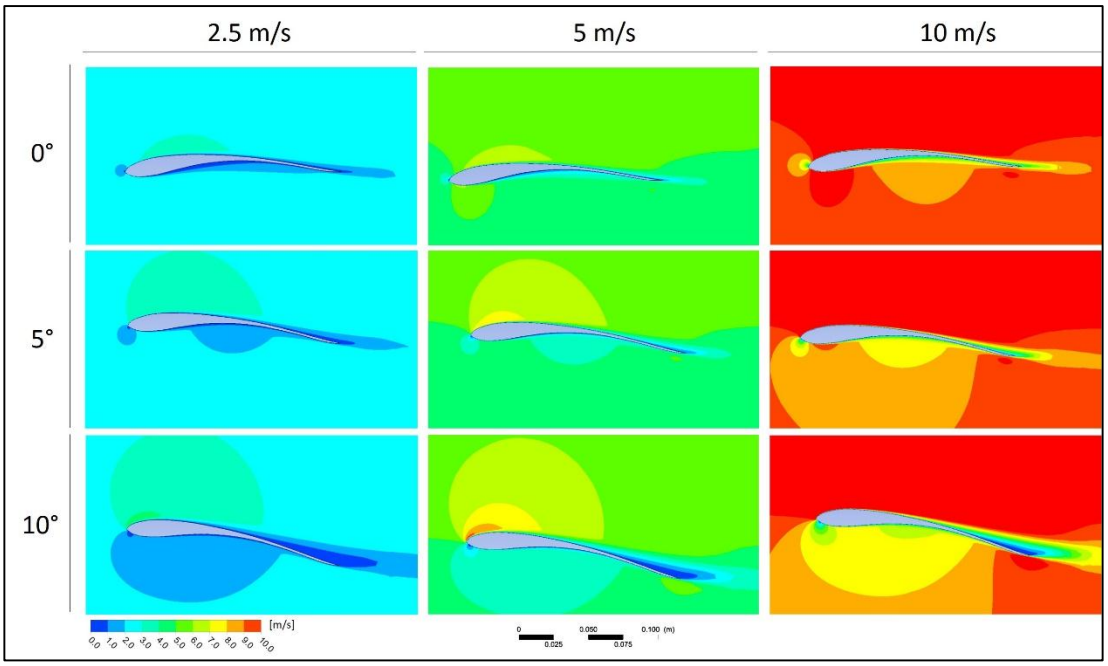

Figure 3.4: Velocity contours for owl airfoil.

However, the falcon airfoil tend to have larger slower regions (0-1 m/s) on the pressure side for all cases. Specifically, the results at 0° AOA have more flow discontinuities compared to the owl (figure 3.5). Since the stationary region lies between 15-65% for the owl (0°-2.5 m/s), despite that for the falcon (0°-2.5 m/s) it is from the leading edge till 75% of the chord. This is a consequence of the differences of the curve radius on the bottom side of the airfoil profile of the two birds. On the other hand, considering the suction side, 0-1 m/s regions are seen for 10° AOA results as like as the 10° AOA results of the owl. For the 10° AOA situations the minimum velocity (0-1 m/s) contours start at 55%, 73% and 76% of chord length respectively, and exceeds the trailing edge.

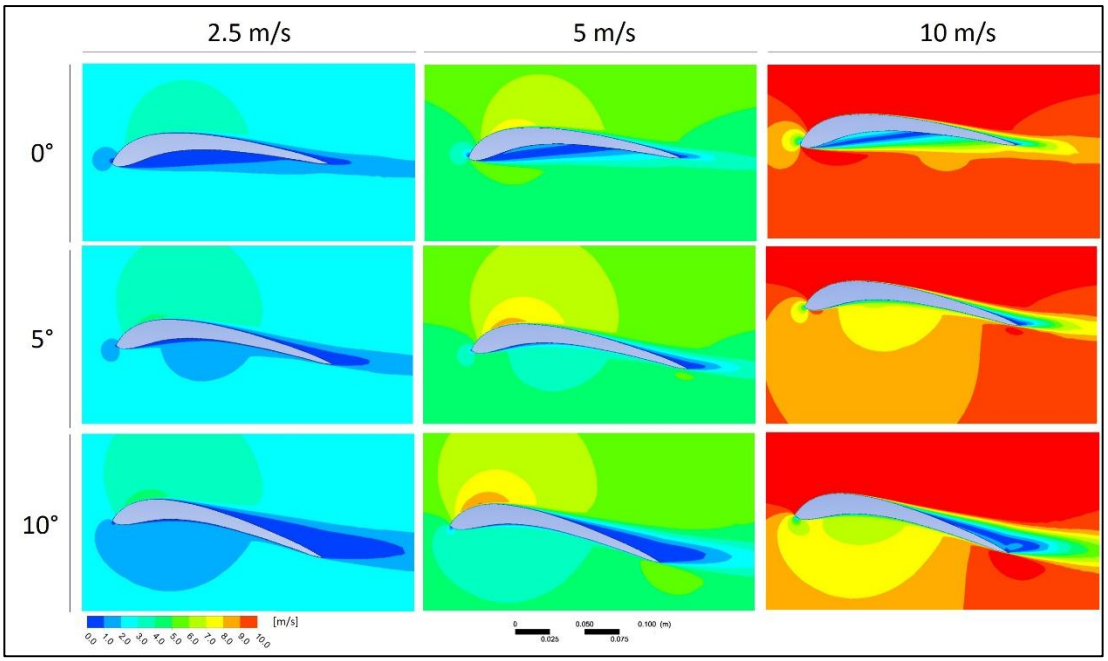

Figure 3.5: Velocity contours for falcon airfoil.

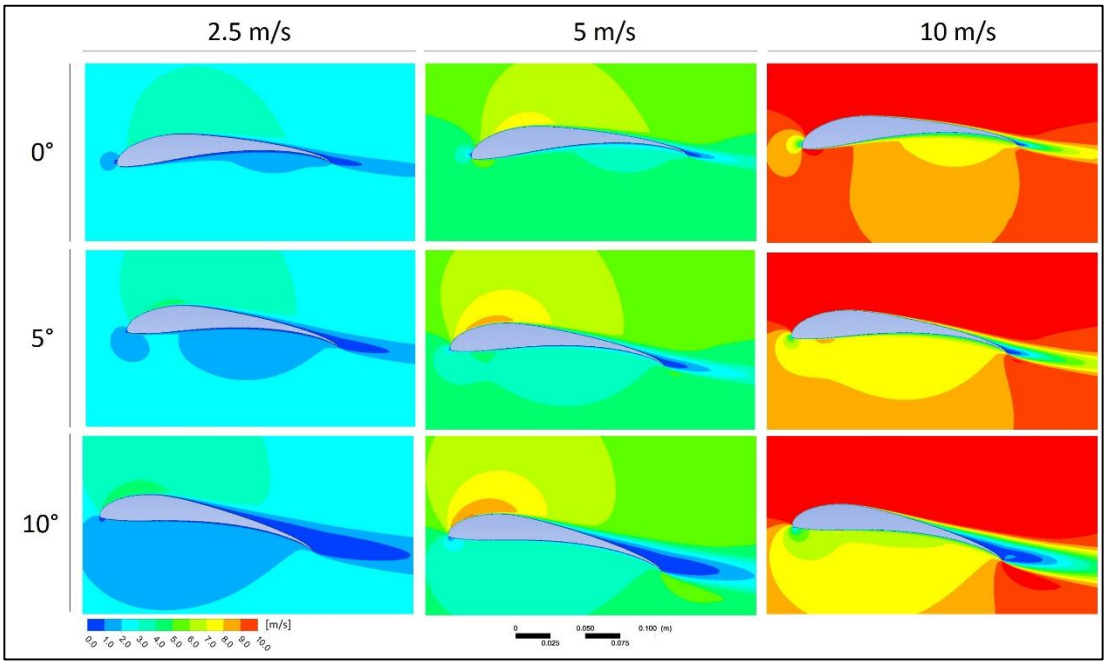

Figure 3.6: Velocity contours for gull airfoil.

By analyzing the gull airfoil (figure 3.6) an important feature stands out on the pressure side, no slow regions are seen. A possible reason for this can be that the rather flat lower side leads to a smoother approach of flow to the airfoil. The minimum velocity regions for 10° AOA remains similar to the other two birds, where the starting point is at 70% for 2.5 m/s, at 82% for 5 m/s and at 88% of the chord for 10 m/s.

3.1.3. Vorticity Distributions

For all velocities and AOA's, the flow over the owl profile stays attached to the airfoil, which can be clearly seen in the vorticity contours in figure 3.7. By considering the AOAs as three subgroups, the vorticity size on both suction and pressure side increases together with the free stream velocity for the subgroups. As shown in the 10 m/s results the positive and negative vorticity regions after the trailing edge have aproximately the same length for all three AOAs. This is not the case for the other velocity conditions. The length of the vortices for 10 m/s doubled from 0° to 5°, and tripled from 0° to 10°, which is expected due to increase in AOA.

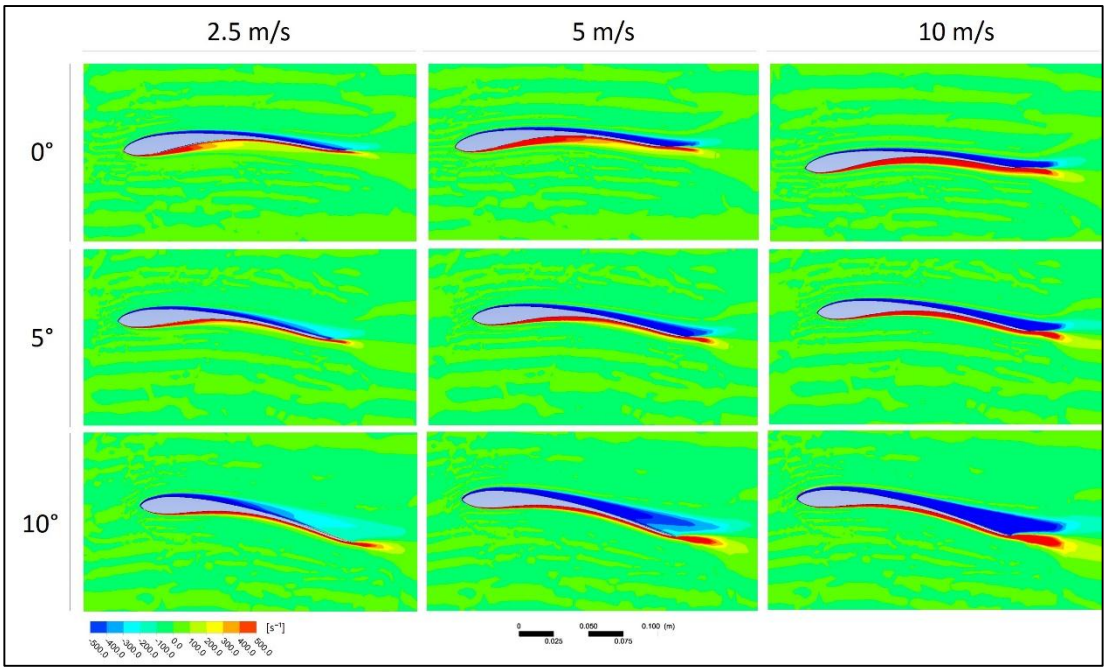

Figure 3.7: Vorticity contours for owl airfoil.

An interesting situation attracts the attention in the falcon results in figure 3.8 at the 0°-2.5 m/s condition, where positive vorticity is seen on the suction side and negative vorticity on the pressure side. This is a vise a versa case compared to the other results, and can be described with the high slope (relative to the owl and gull) on the leading edge of the falcon airfoil. As well as the velocity distributions for the 0° AOA falcon, the vorticity distributions also hint to the flow seperations on the pressure side. Furthermore, as the AOA increases, the flow is tend to separate from the suction side for all three free stream velocities. The vortex lengths of both positive and negative

reaches similar limits after the trailing edge for 5 m/s and 10 m/s, but in general the positive vortices extend to a further limit than the negative vortices. A negligible change in negative vortex length is seen in the 5 m/s case, where the positive vortex length is doubling with the growth in AOA. The same thing can be said for the 10 m/s column, except the 10°-10 m/s case, which shows a drastically increase in vortex length.

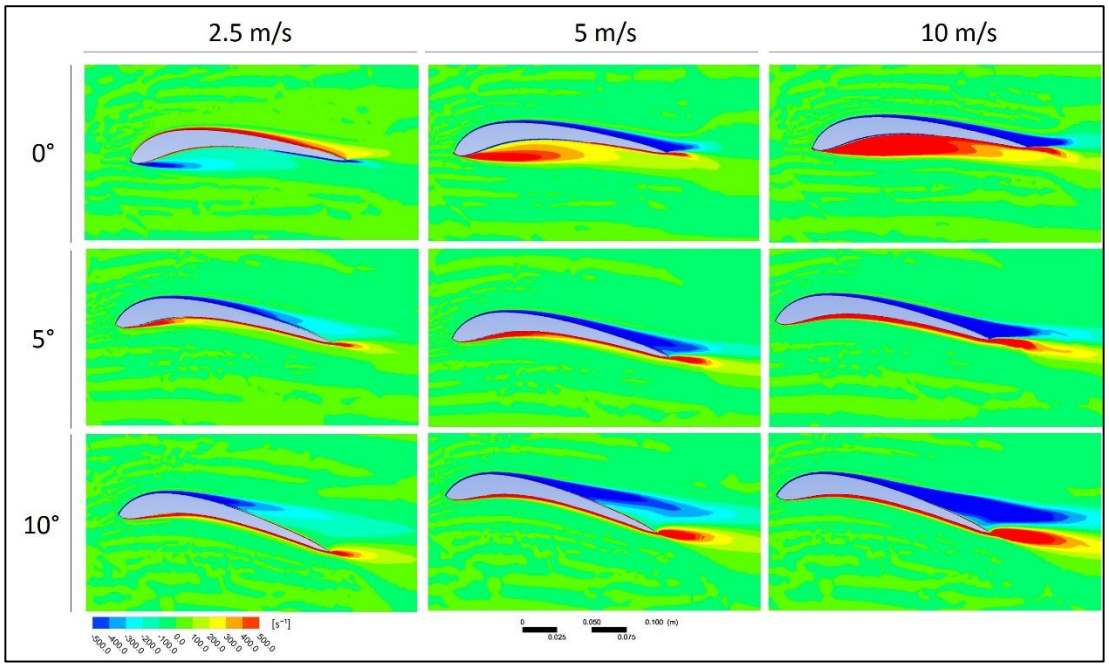

Figure 3.8: Vorticity contours for falcon airfoil.

The gull airfoil (Figure 3.9) lies between the owl and the falcon in terms of general topology of vorticity. The flow is not well attached like in the owl, but it follows the airfoil more than the falcon. Different from them, the positive vorticity length after the trailing edge zone is much thinner and longer. This can maybe a result of the smaller curve on the pressure side relative to the other two airfoils or the trailing edge geometry.

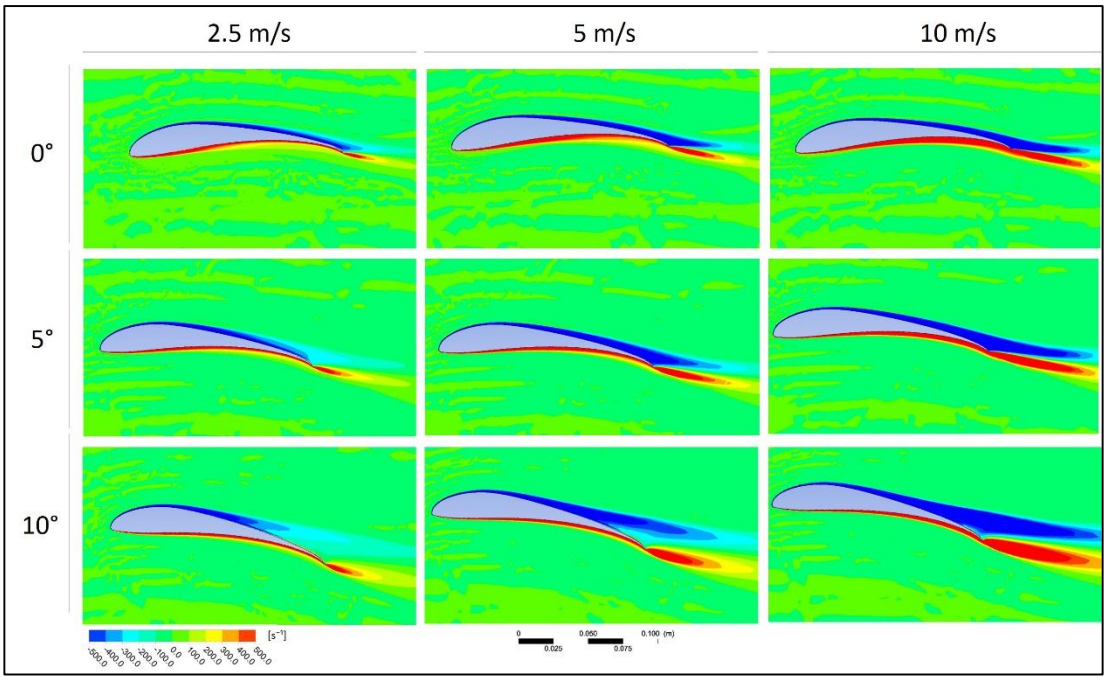

Figure 3.9: Vorticity contours for gull airfoil.

3.2. Transient Results

The steady state results are realized to obtain a general view about the airfoils. In order to understand the acoustic behaviour of each wing profile, a detailed look in the topology of the flow is required, which can be achieved with the transient analyzes. Therefore, the vorticity distributions are investigated in a wider context in this section. The results are shown in 2 groups for every bird wing airfoil. The first group consist of results, where each case is investigated in four equally spaced instant (0.5 seconds between steps), and are mostly periodic cases. The second group contains non-periodic, case spesific events, which are investigated additionally with streamlines.

3.2.1. Owl

The results for free stream velocity of 0°-2.5 m/s (figure 3.10) show that the flow is relatively smooth and the vortices are periodical. Positive vortices form at an early point (compared to 0°-5 m/s and 0°-10 m/s) at the leading edge pressure side, whereas the suction side flow is smooth and mostly attached to the boundary layer. Moving to the 5 m/s column, both the positive and negative vortices grow relative to the 2.5 m/s column. Here, the vortices on the suction side get bigger in diameter. Also at the

trailing edge an interaction between the negative and positive vortices is more clearly. Comparing the two cases (0°-2.5 m/s and 0°-5 m/s) at each time step, the flow pattern looks quite similar, especially the positive vortex pattern. The 10 m/s results contain larger vortices, which is expected due to the increase in velocity. Different from the two previous cases, positive vortices start to affect each other, particularly seen at t=1.0s and t=2.0s near the leading edge (mushroom shape vortex). Positive-negative vortex interaction can be seen on both sides of the airfoil, while at the suction side near the trailing edge positive vortices force the flow to seperate from an earlier point of the airfoil surface. Furthermore, flow interactions intensifies after the flow leaves the trailing edge. Since the owl profile is a highly cambered profile (relative to the gull profile), it is expected that the vortex shedding starts at a point near the leading edge of the profile, especially at small AOA's e.g 0°.

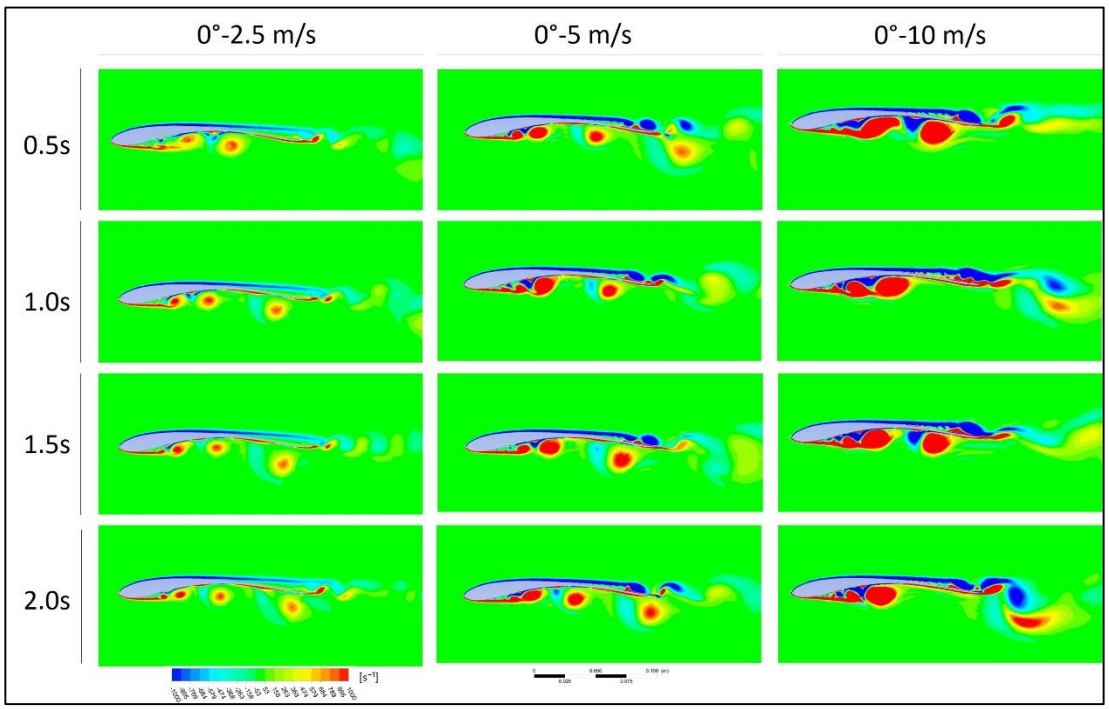

Figure 3.10: Vorticity distributions of AOA=0° for owl airfoil in four equally spaced instants.

Moving further to the results of AOA=5°, the first point that stands out is the seperation of the vortices at approximately the half chord length, whereas for the 0° AOA results the seperation point is closer the trailing edge at approx 75% of the chord (figure 3.11). It can be concluded that this an outcome of the increase in AOA, since the free stream velocity values didn't change. Another outcome of this change is that

the negative vortices start to grow and get even larger than the positive vortices on the pressure side. Looking carefully to the 10 m/s column, on the suction side at 50% of the chord, the negative vortex grows over the positive vortex, and traps it between the airfoils surface. This can be a possible seperation bubble formation in the flow.

Interesting results can also be seen at the trailing edge for the 5° case (figure 3.11), as the positive vortices on the pressure side travels in a vertical direction in first place, and then moving in the same direction as the flow after interacting with the negative vortices. A possible reason can be that the geometry of the owl airfoil's trailing edge is sloping upward. Furthermore, this slope leads to different interactions of vortices, which can effect the acoustic characteristics of the owl wing profile.

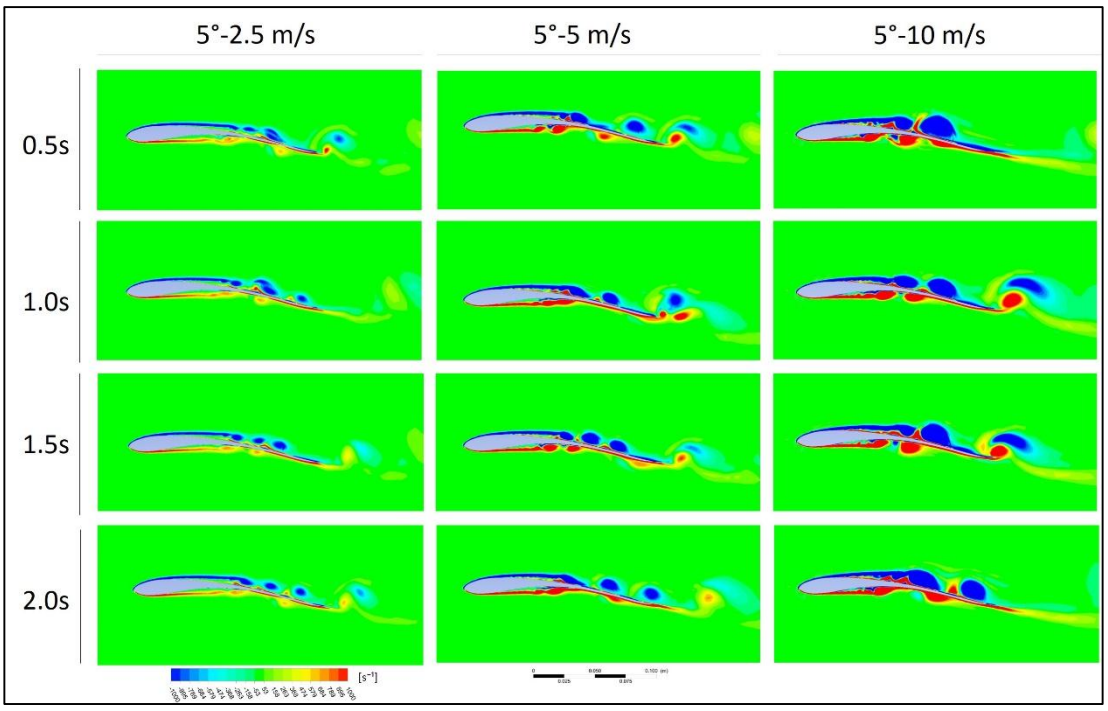

Figure 3.11: Vorticity distributions of AOA=5° for owl airfoil in four equally spaced instants.

For the AOA=10° results in figure 3.22, the seperation point of the negative vortices shifts forward to the leading edge and reaches almost 25% of the chord length. The 10° AOA causes the flow seperate from an earlier point of the airfoil. A similar effect is also seen in the 5° AOA results. The 2.5 m/s column has small vortex shedding, while the 5 m/s and 10 m/s columns show rather greater shedding in the flow. It is clearly seen that the airfoil is better adapted to the flow at 2.5 m/s, because

the flow stays attached at the pressure side, which is a desired situation for airfoils to produce lift, and it is also known that the owl flies slower than the other two birds.

By investigating the vortex dimensions, the diameter doubled from 2.5 m/s to 5 m/s, and almost tripled from 2.5 m/s to 10 m/s. Different from the other two cases, the 10° AOA results demonstrate vortex interactions, which are similar to the previously mentioned as dipole and quadrupole sources. The 10 m/s – 0.5s case in figure 3.22 is an example for dipoles, whereas 10 m/s – 2.0s indicates a quadrupole. These sources are also seen in the 10° - 5 m/s results, while vortices with much smaller diameters are present in the 5° - 5 m/s and 5° - 10 m/s figures.

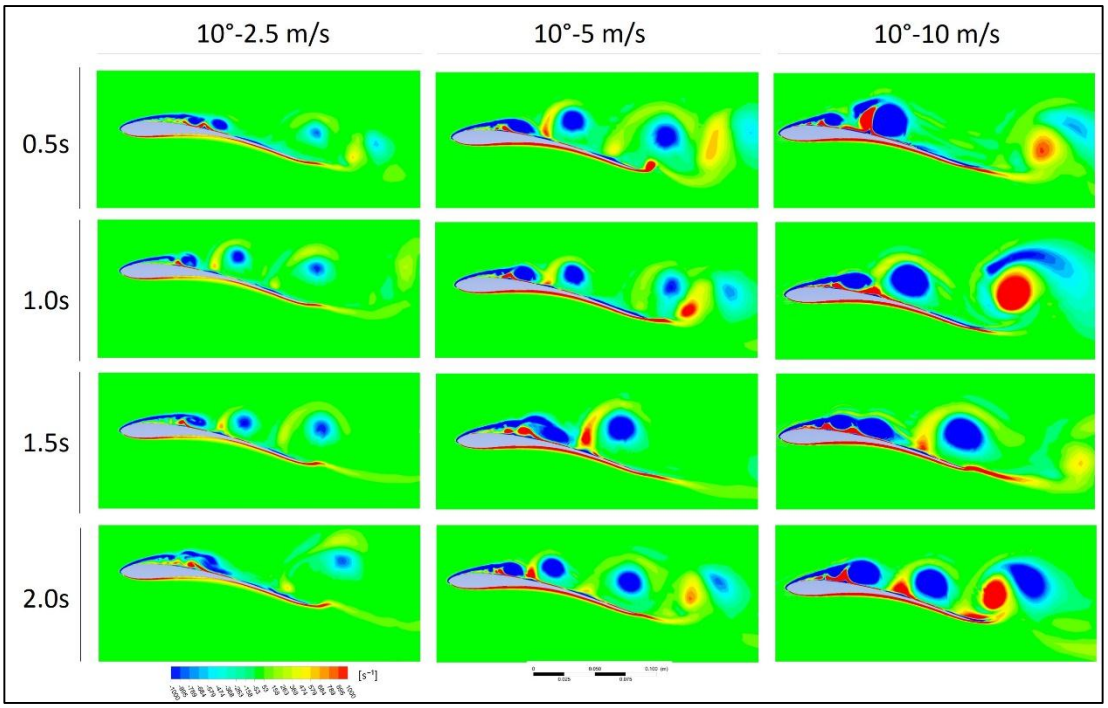

Figure 3.12: Vorticity distributions of AOA=10° for owl airfoil in four equally spaced instants.

3.2.2. Falcon

Starting with the falcon profile geometry, it has a large curve at the pressure side. The effect of this camber can be directly seen in 0° AOA results (figure 3.13), where the flow seperates after a small contact with the wing profile. This leads to formation of vortices in an earlier point at the profile than the other two birds. Further at the suction side, the flow also seperates but stays attached to the airfoil for a longer length, similar to the owl profile. Note that, in the 5 m/s and 10 m/s results the negative

vortices at the suction side tend to merge with each other and generating a larger vortex.

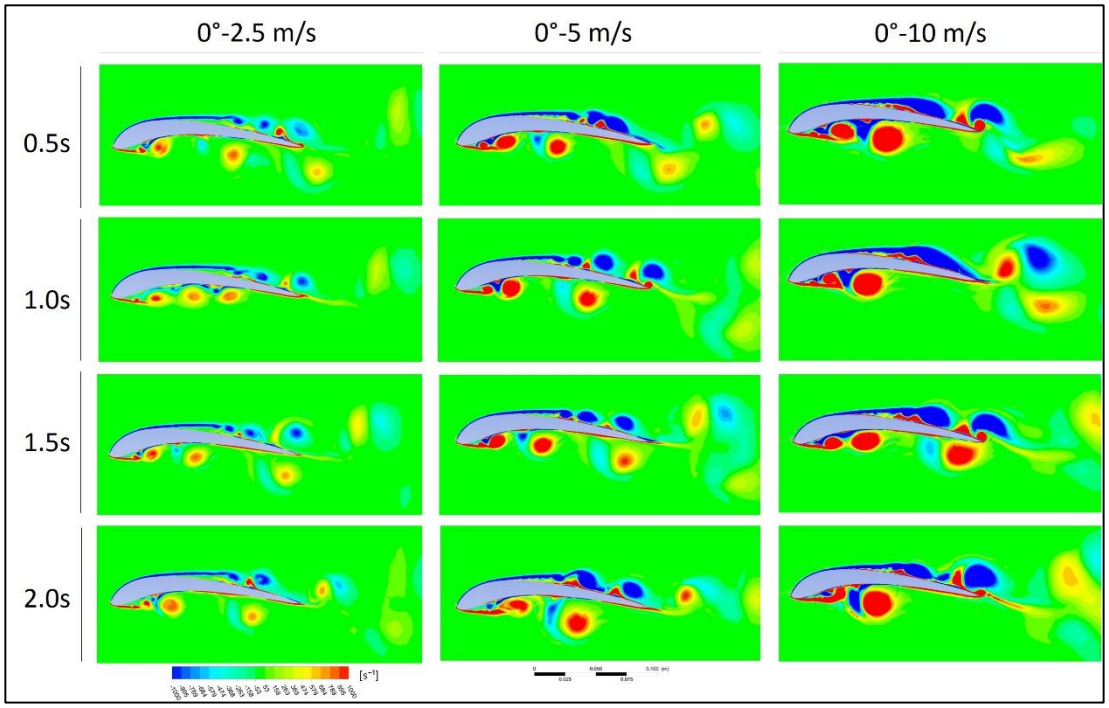

Figure 3.13: Vorticity distributions of AOA=0° for falcon airfoil in four equally spaced instants.

With the increase in AOA to 5°, the flow on the pressure side draws closer to the airfoil and is attached for a longer length (figure 3.14), while the flow on the suction side moves away and seperates from an earlier point at the wing profile. Another case is seen at the trailing edge, especially in the 10 m/s column, where the vortex at the pressure side grows without going into the suction side of the airfoil. This was not the case for the owl profile, since the vortices moved to the suction side occasionally.

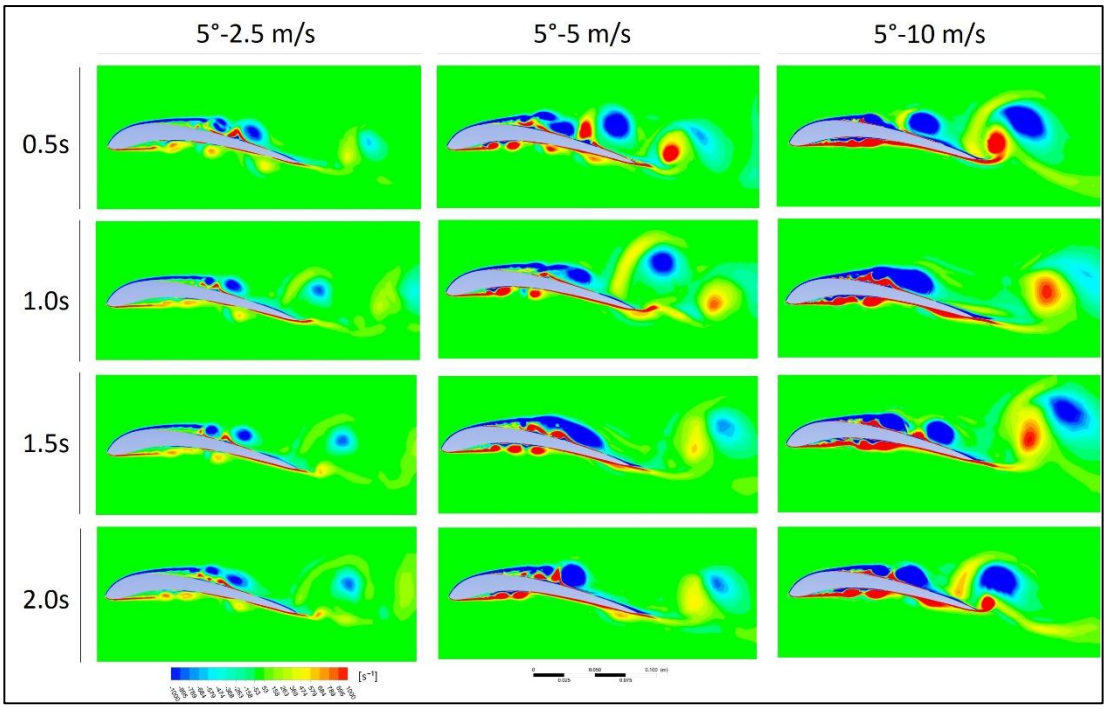

Figure 3.14: Vorticity distributions of AOA=5° for falcon airfoil in four equally spaced instants.

The AOA=10° results in figure 3.15 shows a relatively better flow characteristic at the pressure side compared to Figure 3.13 and 3.14. It is generally smooth and stays attached to the airfoil. The vortices on the suction side continue to merge and grow over the airfoil. This is a possible example for a seperation and attachment of the flow. By mentioning this, the seperation point moves towards the leading edge with increase in AOA, which is approximately at 30% of the chord for 0°, 20% for 5° and 12% for 10°. A notable feature can be seen when the vortex strength is examined. By keeping the AOA at 0°, the vortices getting larger by increasing the free stream velocity, but it is not the same for 5° and 10° AOA results. Therefore, vortices may get larger from 2.5 m/s to 5 m/s, but they are quite similar in size by increasing the velocity from 5 m/s to 10 m/s. A possible reason for this is the merging tendency of the vortices as seen in Figure 3.14 and 3.15. This leads to grow in vortices occasionally for the 5°-5 m/s, 5°-10 m/s, 10°-5 m/s and 10°-10 m/s cases.

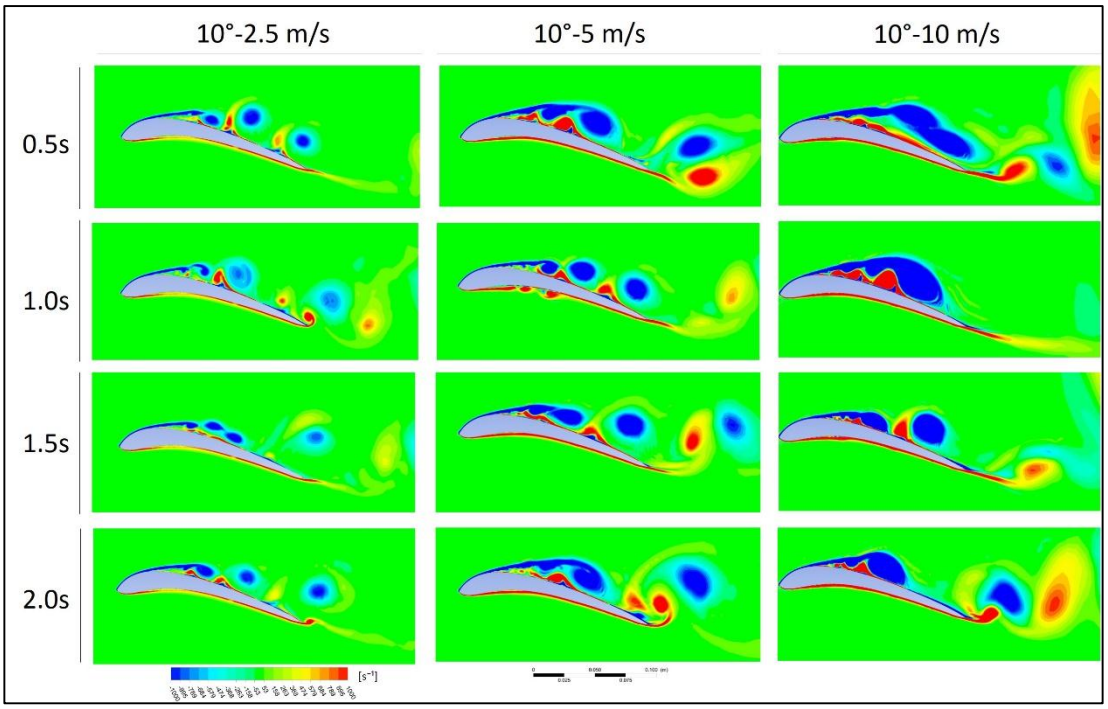

Figure 3.15: Vorticity distributions of AOA=10° for falcon airfoil in four equally spaced instants.

The results for falcon indicates that the flow behaviour shares similarities with the owl results, because of the highly curved geometry (compared to the owl airfoil) on the pressure side of the profiles are alike. Hence, the vortices on the pressure side getting smaller from AOA=0° to AOA=5°, while almost disappear at AOA=10°.

3.2.3. Gull

The 0° AOA results (figure 3.16) for the gull wing profile shows a different behaviour of the flow compared to falcon and owl, especially on the pressure side. For falcon airfoil, the vortices starts to seperate at the half chord length, but in the gull profile results the vortices stays attached for a longer length. In contrast to falcon and owl the flatter pressure side of the gull profile is a potential answer to this issue, which is also a distinctive feature of the gull wing profile.

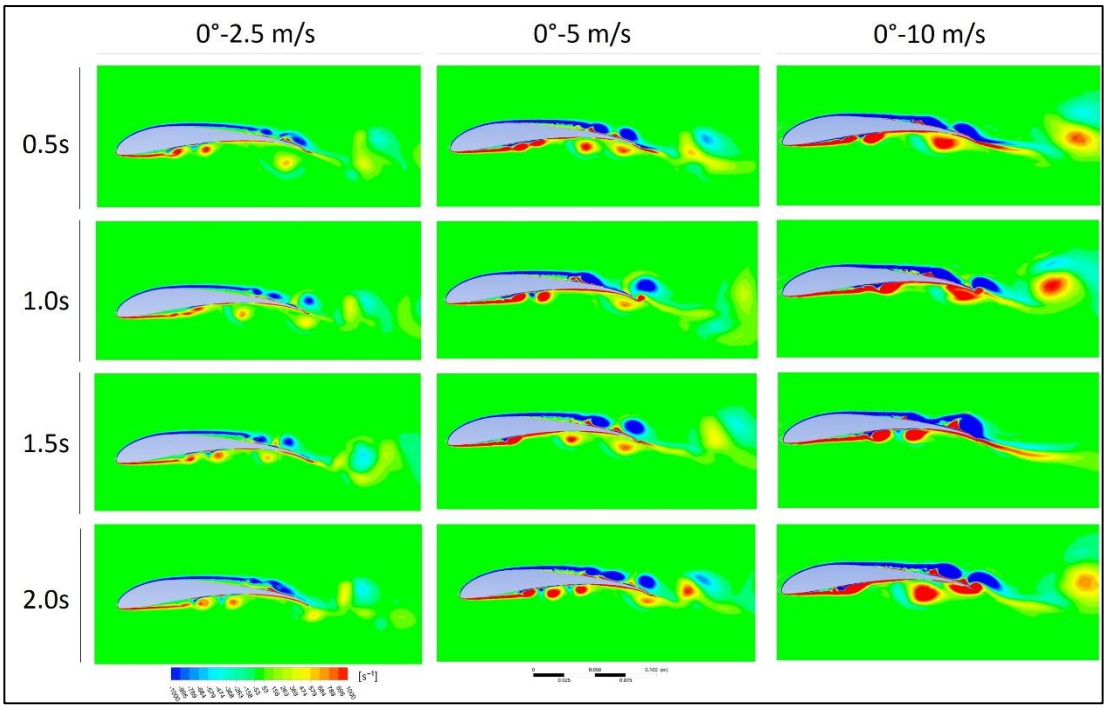

Figure 3.16: Vorticity distributions of AOA=0° for gull airfoil in four equally spaced instants.

In Figure 3.17, again, no vortex shedding is seen at the 5° AOA, same like the 0° AOA. Both 5°-5 m/s and 5°-10 m/s cases have examples for flow seperation and reattachment on the suction side, e.g. t=0.5s and t=2.0s images. The figures also show constant grow rate of the vortices with increase in velocity. Besides that, the trailing edge geometry affects the vortex generation in this area, where the trailing edge is directed downwards (approx. 45°), thus prevents the vortices to going into the suction side from the pressure side.

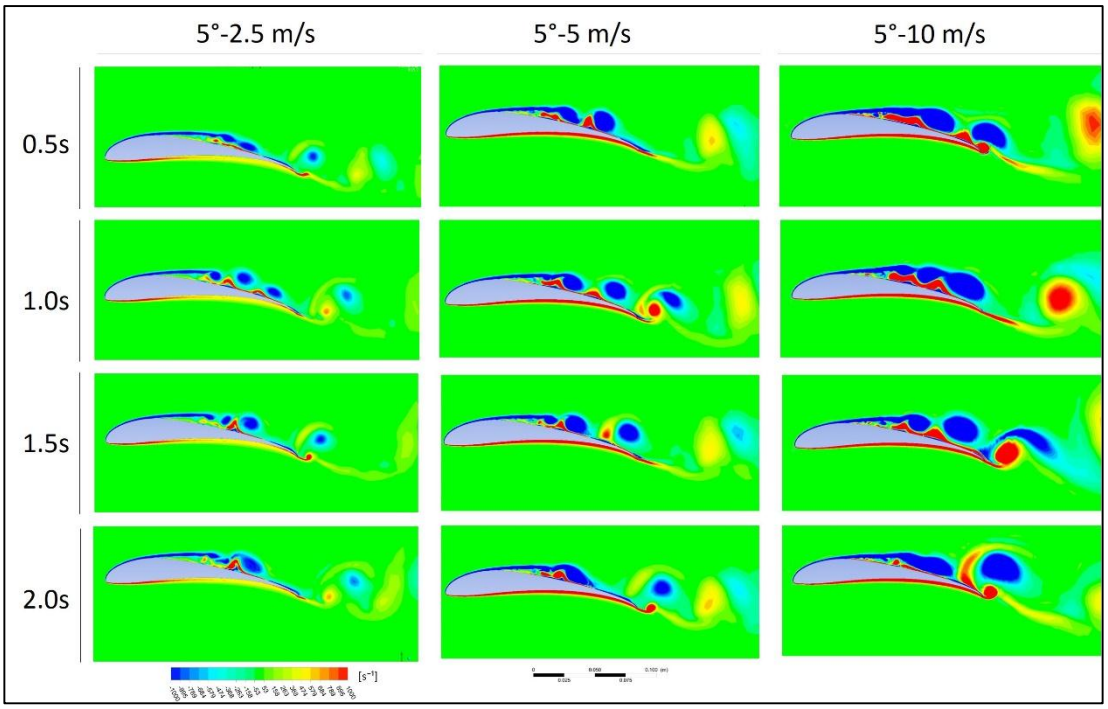

Figure 3.17: Vorticity distributions of AOA=5° for gull airfoil in four equally spaced instants.

By increasing the AOA to 10° (figure 3.18), the seperation point of the flow on the suction side moves forward to the leading edge similar to the other two birds. The seperation point for 0° is almost at the half of the chord length, for 5° it is the 30% of the chord, and for 10° it is 20% of the chord. Furthermore, dipole and quadrupole sound source examples are clearly present in the 10°-10 m/s results, and a noteworthy increase in the vortex diameter is also seen. The vortex diameter is approximately doubled from 2.5 m/s to 5 m/s and doubled again from 5 m/s to 10 m/s.

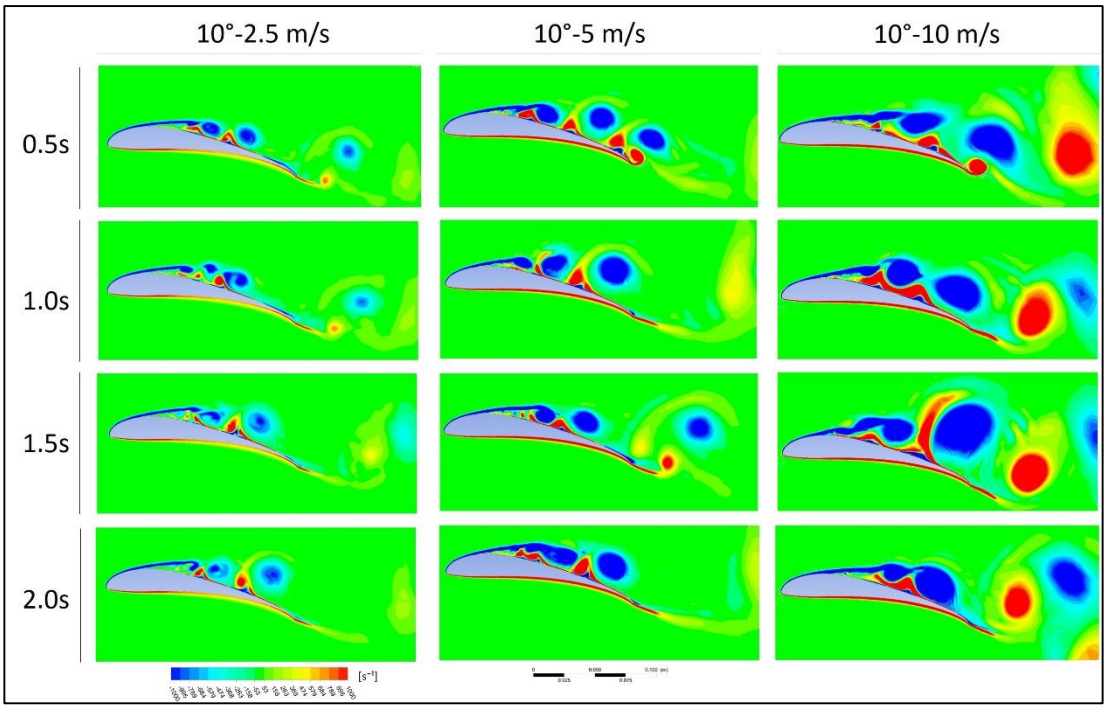

Figure 3.18: Vorticity distributions of AOA=10° for gull airfoil in four equally spaced instants.

3.2.4. Summary of the Results

Till now, the birds were compared crosswise, and both similarities and differences were mentioned in terms of vorticity. Before diving into the acoustic chapter, a brief summary to wrap up the results is thought to be necessary. A general summary together with extra streamline figures to demonstrate the differences are investigated in this section.

Starting with the flow seperation points of each bird, it is found that at maximum AOA and velocity, the locations are at 20-25%, 10-15% and 5-10% of the chord length for gull, falcon and owl respectively. The slope at the leading edge (suction side) of the gull is rather flatter than of the falcon and owl. This flatness can be the reason of this situation. Another difference because of the geometry is seen at the trailing edge, where the slope at the end of each bird profile differs. Looking in detail to Figure 3.19a (streamline), it is seen that the flow is curved vertically for the owl (indicated by the black arrows), since the trailing edge geometry has a slope upwards. In Figure 3.19b, the flow leaves the trailing edge tangent to the airfoil, where in Figure 3.19c it is slightly curled horizontally, because the trailing edge is sloped downwards.

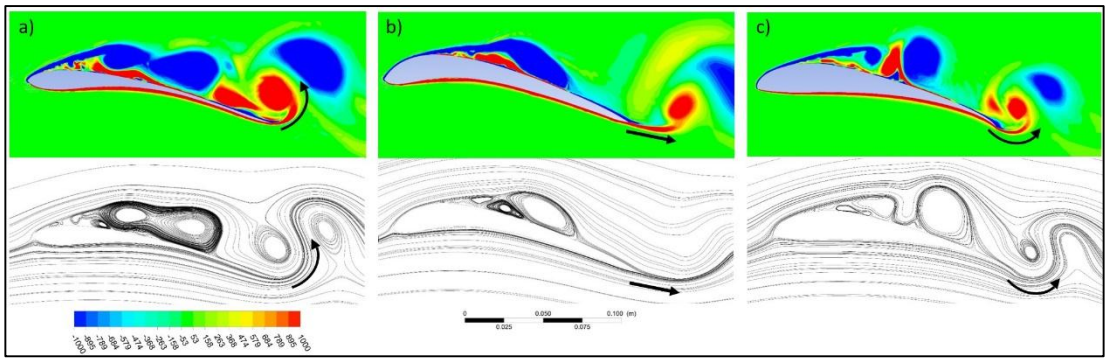

Figure 3.19: Trailing edge vortex direction a) Owl (10°-10m/s), b) Falcon (10°-5m/s), c) Gull (10°-10m/s). The black arrows indicate the first movement of the streamlines just leaving the airfoil.

By increasing the AOA it is seen that all three airfoils affected in terms of the flow on the pressure side. Especially, it is concluded that the gull has a better adapted flow in terms of vortex shedding on the pressure side in all angles (probably because of the flatter pressure side of the airfoil compared to other two birds), while the other two birds shows significant improvement at 10° AOA. A remarkable situation is seen in the falcon results, when the vortices merge with each other. Figure 3.20b shows a merging vortex, which is causing a large wake in the flow. This type of vortices is mostly seen in the falcon but examples also found for the gull and owl. The difference between them is that the large negative vortex on the gull (figure 3.20c) is the farthest away from the airfoil. One reason can be that the largest positive vortices on the suction side formed on the gull wing profile.

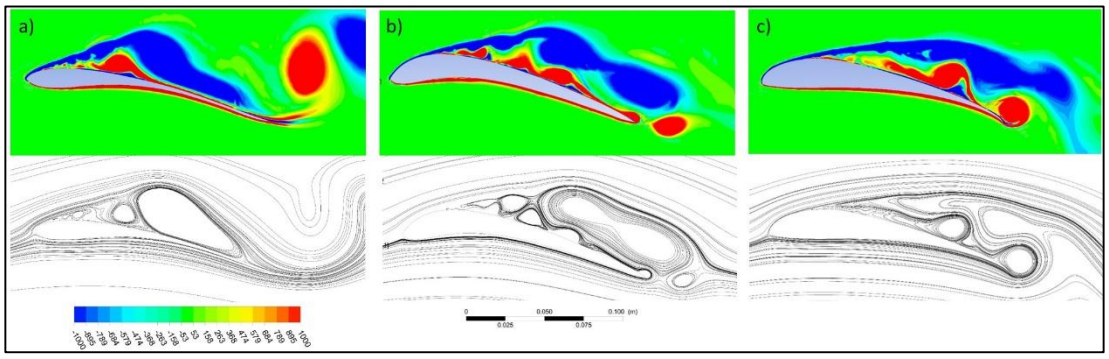

Figure 3.20: Vortex growth over the airfoil a) Owl (10°-10m/s), b) Falcon (10°-10m/s), c) Gull (10°-10m/s).

In general, the figures for all birds show that the 2.5 m/s cases are negligible in terms of acoustics. Rather small vortices are present in the 2.5 m/s free stream velocity results and almost no vortex interactions are seen at all. This can be evaluated as low

sound sources (monopoles, dipoles and quadrupoles). Since the vortices for 5 m/s and 10 m/s are larger, it can be concluded that noise generation is going to be greater compared to 2.5 m/s. Also reviewing the 0° AOA analysis with regarding to aerodynamics, it is concluded that the main source of vortex shedding is located at the pressure side of the related wing profiles. Actually turbulence is unavoidable, but it is more preferred to have a turbulent flow on the suction side, in terms of lift generation. Therefore, from aerodynamic and acoustic point of view, it is decided that the 2.5 m/s and the 0° AOA cases won't be investigated further in the acoustic chapter.

4. ACOUSTIC RESULTS

In this chapter, the results of the acoustic analysis of the owl, falcon and gull are investigated in terms of sound pressure level (dB). As mentioned in the previous chapter, the 5°-5 m/s, 5°-10 m/s, 10°-5 m/s and 10°-10 m/s cases are selected for aeroacoustic investigations for all three type of birds. The aerodynamically generated noise is measured at the receivers, which are placed around the airfoils in a distance of 10 times the chord length (1.5 m). The receiver order starts at trailing edge (0° receiver), and continues in a counter-clockwise direction with 20° increments (figure 4.1). First, the acoustic data at the 0° receiver (figure 4.1) is investigated to find the maximum sound pressure level in a range between 0-7500 Hz for all birds. After that, the maximum sound pressure level (SPL) is examined together with the remaining 17 receivers in a radar chart. The frequency interval in the radar charts corresponds to the maximum SPL range.

To be able to understand the acoustic charts in this chapter, the meaning of the reference acoustic pressure must be known. It is defined as the threshold of hearing for humans and has the value of $2x10^{-5}$ Pa (=0 dB) [57]. The negative sound pressure levels should be understand as values, which are below the reference acoustic pressure.

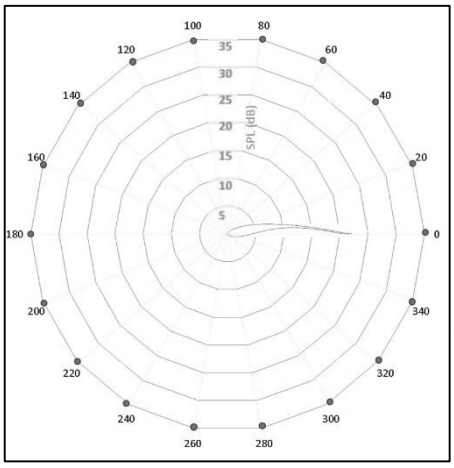

Figure 4.1: 360° receiver positions around airfoil. Each receiver is 1.5m away from the leading edge.

4.1. Acoustic Results at the 0° Receiver

The following figures in this section show the results for the 5°-5 m/s, 5°-10 m/s, 10°-5 m/s and 10°-10 m/s cases for each bird, while the frequency range is between 0 - 7500Hz. In figure 4.2, the maximum sound pressure level (SPL) for the birds are almost at the same level, in a frequency interval of 20 - 120 Hz with a maximum SPL of 22dB for falcon and gull, and 17dB for owl. After approx 400 Hz, the curve of the three birds starts to split from each other until the falcon and gull unite around 2250 Hz. On the other hand, the owl keeps it distance nearly constant at 10dB to the other two birds.

By increasing the velocity to 10 m/s (figure 4.3), the SPL rises up to almost 40dB. Here, the maximum SPL propagates to a wider frequency range of 90 – 290 Hz. Between 0 – 3000 Hz the falcon SPL curve tends to approach to the owl curve, while after 3000 Hz it gets closer to the gull curve. The split of the bird curves lies around 750 Hz in this case, which is higher in terms of SPL and frequency compared to figure 4.2. In both figures the owl stands out as the most silent bird, whereas the gull is the most noisy one.

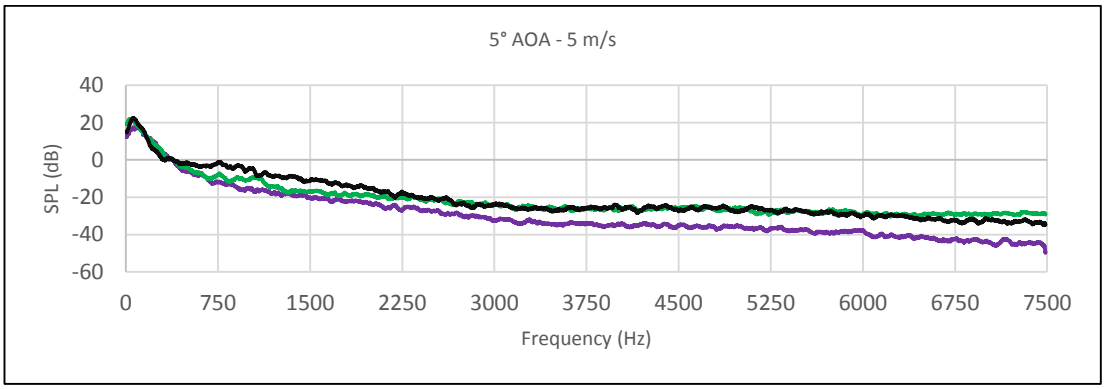

Figure 4.2: Sound pressure level between 0-7500 Hz for 5° AOA -5 m/s flow velocity. Receiver is located at the trailing edge (0°). Owl (purple), Falcon (green), Gull (black).

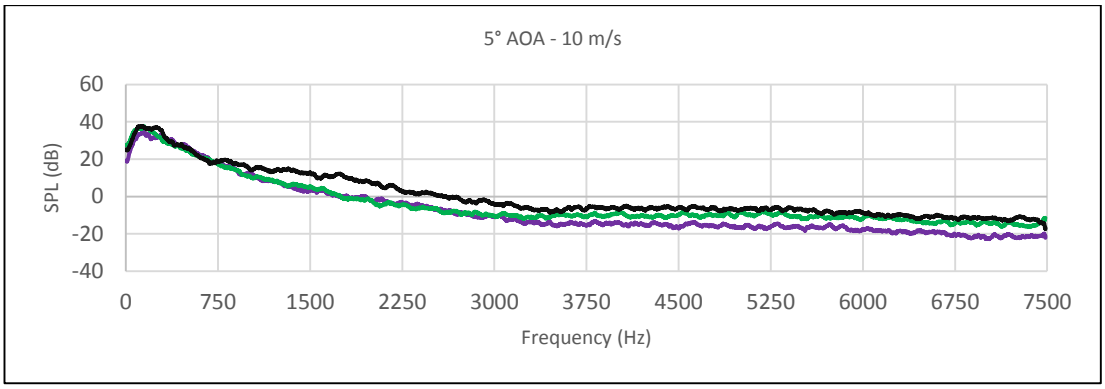

Figure 4.3: Sound pressure level between 0-7500 Hz for 5° AOA -10 m/s flow velocity. Receiver is located at the trailing edge (0°). Owl (purple), Falcon (green), Gull (black).

In figure 4.4 and 4.5 the AOA is increased to 10°, where the effect of AOA on SPL can be seen. The max SPL in figure 4.4 is around 25dB at a frequency range about 15-60 Hz. The curves split at nearly 220 – 250 Hz, but cross each other at 2250 Hz. This shows that between 0 – 2250 Hz the sound generated by the owl is less than the other two birds, but after 2250 Hz the situation changes, and the sound generated by the owl is more. Also in this case, the falcon SPL values are between the owl and gull curves. Between 300-1200 Hz in figure 4.4, an unusual peak in the data is noticed for gull, which will be investigated later in section "4.2 Acoustic Results for 360° Receiver Arrangement".

Interesting results are obtained in the AOA=10° (figure 4.5), where all the curves are layered over each other. Slight differences can be seen, but in general the noise generated by all three birds are pretty much at the same level and follow a similar trend. Also the passing point of the threshold SPL (0dB) is located around 2250 Hz. However, with these results it is concluded that the acoustic advantage (silent flight) of the owl is lost towards the other birds at AOA=10°, especially at 10 m/s free stream velocity.

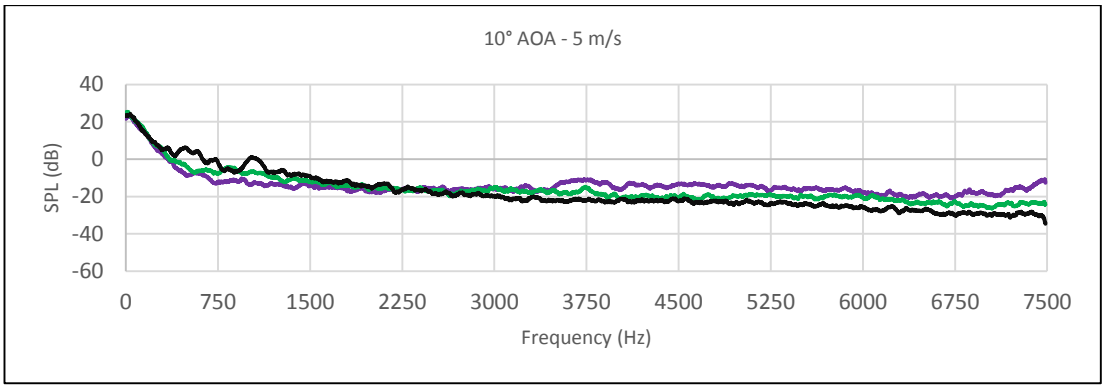

Figure 4.4: Sound pressure level between 0-7500 Hz for 10° AOA -5 m/s flow velocity. Receiver is located at the trailing edge (0°). Owl (purple), Falcon (green), Gull (black).

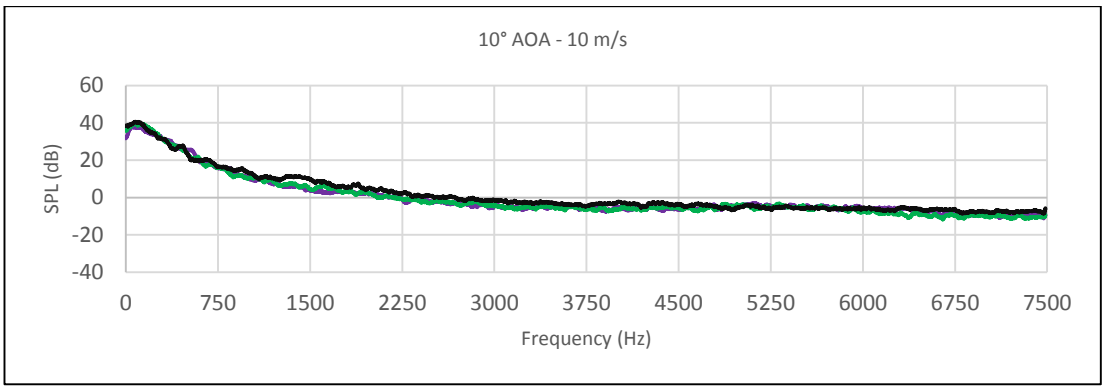

Figure 4.5: Sound pressure level between 0-7500 Hz for 10° AOA -10 m/s flow velocity. Receiver is located at the trailing edge (0°). Owl (purple), Falcon (green), Gull (black).

To sum up the acoustic characteristics of the three birds, it can be said that the owl generates the least noise at 5 m/s free stream velocity regardless the AOA, effectively in a frequency range between 0 – 2250 Hz. In return, the gull tends to create the most noise during flight especially at AOA=5°. On the other hand, the falcon is in between those two in terms of SPL. This can be explained as the falcon airfoil shows better adaptation to these free stream velocities and AOAs.

A general trend in the figures catch the eye between 200-750 Hz. The splitting points of the three curves are similar for the 5 m/s (at approx. 250 Hz) and 10 m/s (at approx. 750 Hz) cases. Considering this, the slope of the figures, which corresponds to the 0-250Hz and 0-750Hz parts of the figures, show a relation to the free stream velocity. So that, the slope for figure 4.2 and 4.4 is around 30°, and for figure 4.3 and 4.5 it is around 50°. This can be explained that vortices with similar characteristics have close formation frequencies for all three birds at this range. Furthermore, the

maximum values in all figures are seen at low frequencies. A possible explanation can be that the free stream velocity is not high enough to form high frequency vortices or the AOA is too small to shed vortices in higher frequencies.

The results of the owl are compared with the literature. Liu et al. [43] found the max SPL (25-30 dB) at around 192 Hz for the similar owl airfoil in a numerical analysis, which verifies the results in this study. Also the max SPL distribution at 10 m/s free stream velocity for an owl airfoil obtained numerically by Li et al. [39] (23-40 dB) is close to the 10 m/s owl case in figure 52 and figure 53, where the values are between 30-45 dB. The slight differences can be related to the dimensions of the airfoil, where Li et al. used 100 mm as the chord length, whereas the chord length in our case is 150 mm. The experimental results in the study of Sarradj et al. [60] shows that the max SPL for the owl and hawk are around 20 dB at regular flight speeds. This can be compared with the 5 m/s data of this study, because the regular flight speed for the owl is max 7.5 m/s. The values in this work varry between 15-30 dB, which is an acceptable deviation for this work.

4.2. Acoustic Results for 360° Receiver Arrangement

In this section, the 360° acoustic results are presented, which are average SPL values for the maximum frequency interval of the three birds. These values are calculated to smooth out the fluctuating data at the maximum frequency interval, and are referred as overall sound pressure levels (OSPL) in this study. The max frequency intervals were mentioned in the previous section, where the range for 5°AOA - 5 m/s is 20 – 120 Hz (figure 46a), for 5°AOA - 10 m/s is 90 – 290 Hz (figure 46b), for 10°AOA - 5 m/s is 15 – 70 Hz (figure 47a) and for 10°AOA - 10 m/s is 40 – 170 Hz (figure 4.7b).

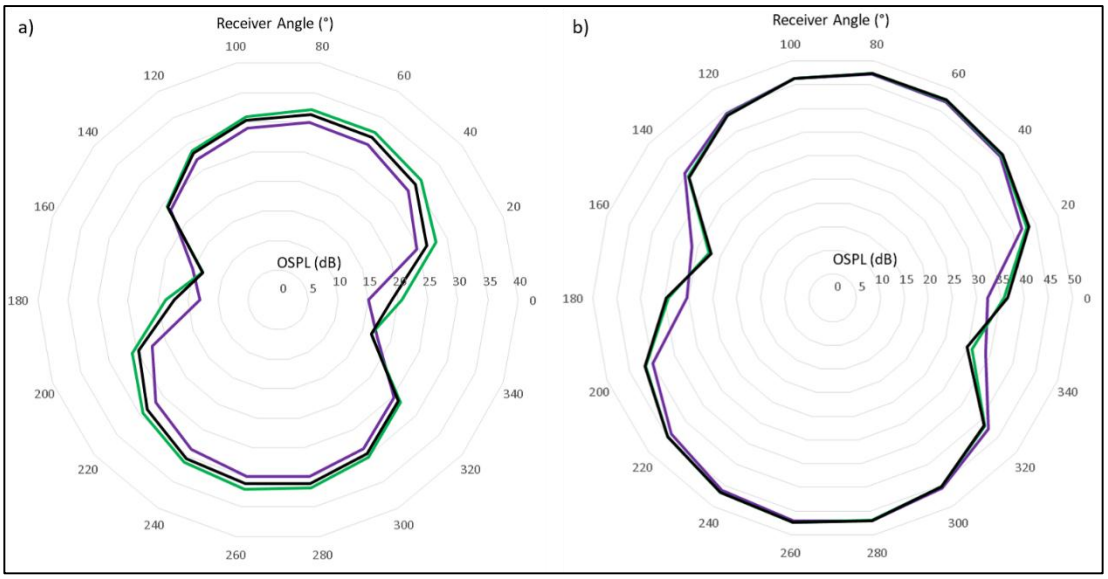

Figure 4.6: 360° OSPL distribution for Owl (green), Falcon (purple) and Gull (black). 18 receivers are equally placed around the airfoil. a) 5°AOA - 5 m/s, 20 – 120 Hz. b) 5°AOA - 10 m/s, 90 – 290 Hz.

Figure 4.6 shows the distribution for the AOA=5° cases. In figure 4.6a, the falcon comes forward as the highest sound generating bird in general. Actually, the OSPL trend is really close to the gull, but in general a 2-3dB offset is seen between the two birds. Despite that, the owl has a similar offset of 2-4dB with the gull, which makes it the lowest overall noise generating bird for this frequency interval. Thus, it can be said that the OSPL's lies between 26-28dB for owl, 29-31dB for gull and 30-33dB for falcon.

With the increase in velocity in figure 4.6b, the OSPL increases directly for all bird airfoil types. Almost no differences are present, which shows that the radiated sound from all three birds are close to each other. Furthermore, the OSPL reaches 45dB, whereas an increase of approx 15dB compared to the AOA=5°-5 m/s case is observed.

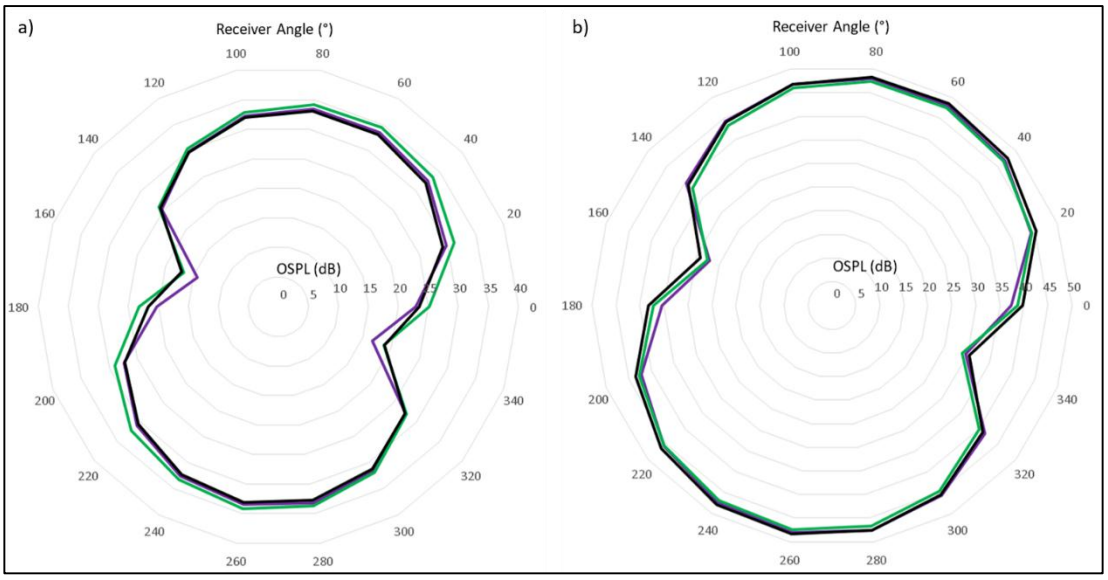

Figure 4.7: 360° OSPL distribution for Owl (green), Falcon (purple) and Gull (black). 18 receivers are equally placed around the airfoil. a) 10°AOA - 5 m/s, 15 – 70 Hz. b) 10°AOA - 10 m/s, 40 – 170 Hz.

For the 10°AOA - 5 m/s (figure 4.7a) case, it can be said that a 5dB increase in contrast to figure 4.6a is noticed as a result of a wider AOA (10°). Again, the falcon is the most noise generating bird as same as in figure 4.6a, while an overlap in the OSPL's for the gull and owl curves are seen. In figure 4.7b, the values are almost overlapped for all three birds, which indicates that at 10° AOA – 10 m/s conditions, any advantage or special feature (e.g. airfoil geometry) for the related birds disappear.

As an overview of the four figures, between the 0°-340° (at trailing edge pressure side region) and 140°-160° (at leading edge suction side region) receivers, a overlap is noticed. A possible explanation can be that the flow causes similar effects at these receivers when entering and leaving the airfoils. It is known that the owl has a max flight speed about 7.5 m/s, which was also mentioned before in this study. Consequently, the OSPL behaviour in figure 4.6b and 4.7b demonstrated that the owl lost its speciality as the least sound generating bird in 10 m/s free stream velocity conditions. Moreover, as a general statement, it can be said that the falcon has the max OSPL at the given frequency intervals.

Except some small disturbances in the acoustic data in section "4.1 Acoustic Results at the 0° Receiver", an unusual situation appeared in figure 4.4 between 300-1200 Hz. Figure 48a is the case, that is mentioned in figure 4.4, which also be taken as reference in the comparisons.

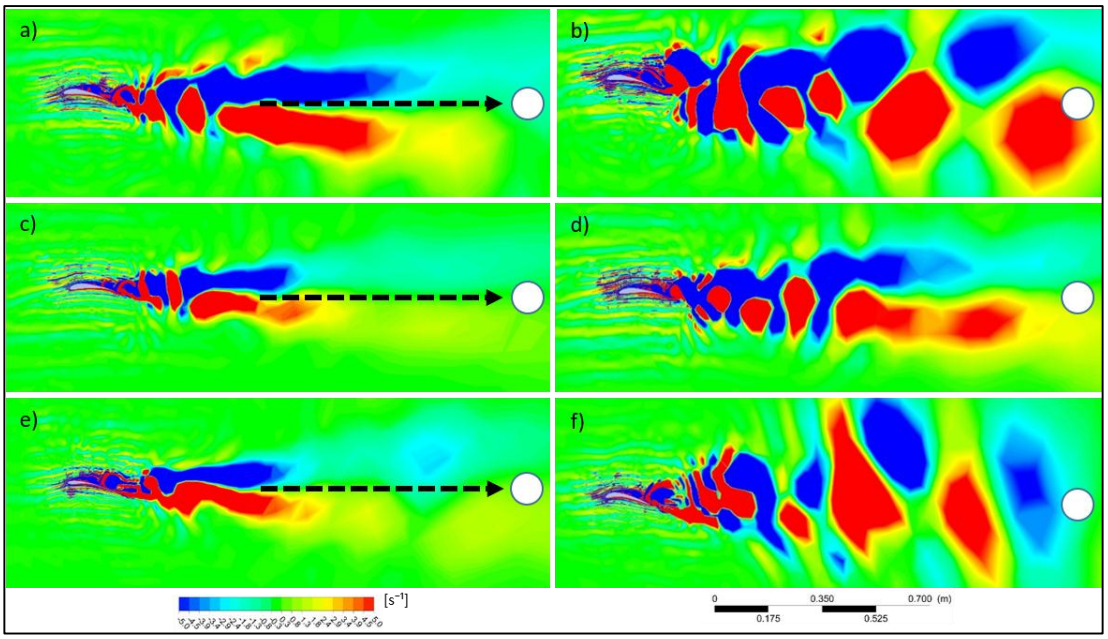

Figure 4.8: Vortex results in far-field for a) Gull AOA=10°-5 m/s, b) Gull AOA=10°-10 m/s, c) Gull AOA=5°-5 m/s, d) Gull AOA=5°-10 m/s, e) Owl AOA=10°-5 m/s, f) Falcon AOA=10°-5 m/s. The white point indicates to the 0° receiver at the trailing edge, where the black arrow shows the focusing direction of the long vortices.

Starting to investigate the topology of the vortices, the left side of figure 4.8 (a,c,e) has rather longer vortices, whereas on the right side (b,d,f) the vortices are shed more frequently. It is considered that the long vortices create a focusing effect like an air channel towards the receiver (white circle in figure 4.8). On the other hand, the focusing effect can't be seen in the shed vortices (figure 4.8b, d, f), and vortices are more distributed to the far-field. Therefore, it is expected that in the long vortex cases, at least for figure 4.8a, the sound pressure level at 0° receiver and in the nearest receivers should be relatively higher than the distributed vortex cases.

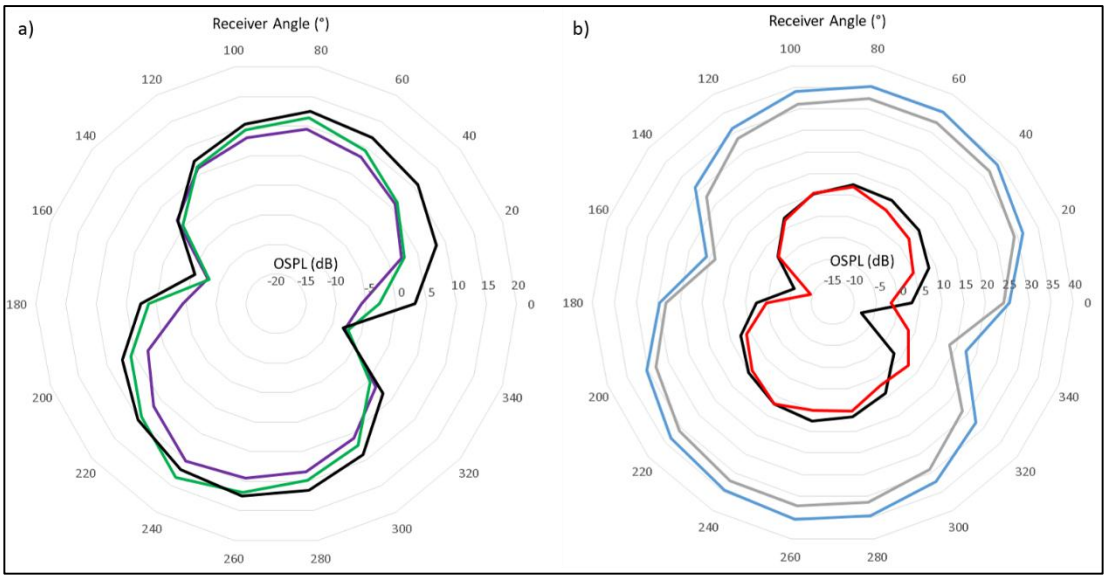

Figure 4.9: 360° OSPL distribution for an interval of 300-750 Hz. a) AOA=10°-5 m/s results for Owl (green), Falcon (purple) and Gull (black), b) Results for Gull AOA=10°-5 m/s (black), AOA=10°-10 m/s (gray), AOA=5°-5 m/s (red), AOA=5°-10 m/s (blue).

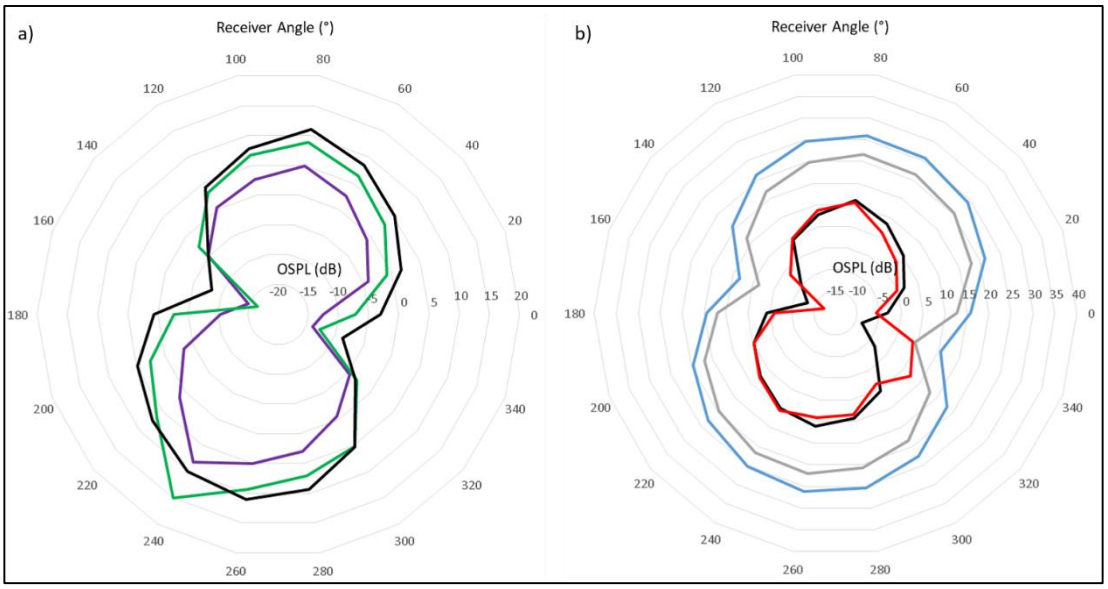

Figure 4.10: 360° OSPL distribution for an interval of 900-1200 Hz. a) AOA=10°-5 m/s results for Owl (green), Falcon (purple) and Gull (black), b) Results for Gull AOA=10°-5 m/s (black), AOA=10°-10 m/s (gray), AOA=5°-5 m/s (red), AOA=5°-10 m/s (blue).

The 300-750 Hz interval in figure 4.9a has a visible increase in OSPL at the 0°, 20° and 40° receivers for the gull (in black). This is an important point, since it was also considered in the vorticity results. The owl has a slightly lower OSPL distribution around 5-10 dB, but it is really close to the falcon at the leading edge suction side. The

falcon OSPL is quite close the gull, which means that the distribution of vortices doesn't really influence the noise generation at all. In figure 4.9b, a relative big gap between the 10 m/s and 5 m/s SPL is seen. Because of that any direct comparison between them would not be meaningful, but in general an unusual value is not observed at the 10 m/s cases. Furthermore, a similar difference in OSPL for the AOA=10°-5 m/s (black) case, which was seen in figure 4.9a, is noticed in figure 4.9b. This again is a sign of the vortex focusing effect idea mentioned before. What can't be explained with the vorticity results in this study is the increase in AOA=5°-5 m/s (red) at the 320° and 340° receivers. This must be investigated further. For 900-1200 Hz interval in figure 4.10, no eye catching result is examined, which relates to this case.

Summing up all the findings in this section, the topology or the characteristics of vortices affect the sound pressure distribution in different ways. Both similarities and differences were present between the birds, even within the same type of bird itself. It is also examined that the owl shows a better "nearly silent flight" feature than the other two birds, which was the expectation of this study. To made distinctive statement about the falcon and gull is hard, because they showed significant similarities throughout the investigations. These results also may shed a light to the peak value in the AOA=10°-5 m/s case for the gull (figure 4.4), but it is not fully proven with the results examined in this study. It needs to be investigated further.

5. CONCLUSION

The objective of this study is to investigate the flow characteristics of birds with their effect on the generated noise. Therefore, typical values that describe the properties of the selected avians are choosen and analyzed with 2D computational fluid dynamics. Three birds, owl, falcon and gull, are selected according to their flight types. Free-stream velocities are 2.5 m/s, 5 m/s and 10 m/s, whereas angle of attacks are 0°, 5° and 10°. Adding together, totally nine cases for each airfoil are investigated in accordance with pressure, velocity and vorticity contours.

The results for the pressure contour show that the camber and trailing edge geometries of the avians have a huge impact on the pressure distribution. Similarities can be seen between the falcon and the owl, while the gull differs from them because of a more flat airfoil. The 10° contours also realize that the trailing edge shape of the gull lead to a higher pressure drop than the other two birds. Velocity contours shed a light to the flow separations of the bird profiles. Here we saw that the camber of the owl and falcon airfoils can cause separations on the pressure side, which is not the case for the gull. On the other hand, the separation points on the suction side are much closer to the leading edge for the falcon compared to the owl and the gull. However, it can be said that the flow on the suction side mostly stayed attached to the boundary layer for the owl, which was a remarkable feature.

The steady state results for the vorticity distribution are realized to obtain a general view about the airfoils. In order to understand the acoustic behaviour of each wing profile, transient analyses are carried out. For the transient results, all three airfoils are affected with an increase in the AOA in terms of flow on the pressure side. Especially, it is concluded that the gull has a better adapted flow in terms of vortex shedding on the pressure side in all angles, while the other two birds shows significant improvement at 10° AOA. A detailed look in the flow seperation points of each bird showed that at maximum AOA and velocity, the locations are at 20-25%, 10-15% and 5-10% of the chord length for gull, falcon and owl respectively. In general, the figures for all birds show that the 2.5 m/s and 0° AOA cases are negligible in terms of acoustics. Rather small vortices are present and almost no vortex interactions are seen at all. Since the vortices for 5 m/s and 10 m/s are larger, it can be concluded that noise generation is going to be greater compared to 2.5 m/s.

The main focus of this study is the acoustic behaviour of the three birds. For the owl, it can be said that it generates the least noise at 5 m/s free stream velocity regardless the AOA, effectively in a frequency range between 0 – 2250 Hz. In return, the gull tends to create the most noise during flight especially at AOA=5°. On the other hand, the falcon is in between those two in terms of SPL. This can be explained as the falcon airfoil shows better adaptation to these free stream velocities and AOAs. By investigating the acoustic results for the 360° receiver arrangement, it is seen that the three birds has a similar sound distribution at the trailing edge (at 0° and 340° receivers) and leading edge (at 140° and 160° receivers). It is known that the owl has a max flight speed about 7.5 m/s, which explains why it lost its speciality as the least sound generating bird in 10 m/s free stream velocity conditions. To made distinctive statement about the falcon and gull is hard, because they showed significant similarities throughout the investigations, but in general, the owl shows a better "nearly silent flight" feature than the other two birds, which was the expectation of this study.

REFERENCES

[1] Arnold M. K., Schetzer J. D., (1959), "Foundations of Aerodynamics", 2nd edition, John Wiley & Sons Inc.

[2] Abdulrahim M., Lind R., (2004), “Flight Testing and Response Characteristics of a Variable Gull-Wing Morphing Aircraft”, AIAA Guidance, Navigation, and Control Conference and Exhibit, Providence, Rhode Island, 16-19 August.

[3] Agrawal B. R., Sharma A., (2016), "Numerical Investigations of Bio-Inspired Blade Designs to Reduce Broadband Noise in Aircraft Engines and Wind Turbines", 54th AIAA Aerospace Sciences Meeting, 4-8 January.

[4] Anderson J. D., (2001), "Fundamentals of Aerodynamics", 3rd Edition, McGraw-Hill

[5] Ansys Inc, (2009), "Ansys Fluent 12.0 Theory Guide", Release 12.0.

[6] Bachmann T., Blazek S., Erlinghagen T., Baumgartner W., Wagner H., (2012), "Barn Owl Flight", Nature-Inspired Fluid Mechanics, 119, 101–117.

[7] Bachmann T., Mühlenbruch G., Wagner H., (2011), "The barn owl wing: An inspiration for silent flight in the aviation industry", Bioinspiration, Biomimetics, and Bioreplication, 7975.

[8] Bachmann T., Wagner H., Tropea C.,(2012), "Inner vane fringes of barn owl feathers reconsidered: morphometric data and functional aspects", Journal of Anatmoy, 221, 1-8.

[9] Bachmann T., Winzen A., (2015), "Owl Inspired Silent Flight", Handbook of Biomimetics and Bioinspiration, Chapter 26.

[10] Batchelor G., (2000), "Introduction to Fluid Mechanics", Cambridge University Press.

[11] Baumel J.J., (1993), "Handbook of Avian Anatomy: Nomina Anatomica Avium", 2nd Edition, Nuttall Ornithological Club.

[12] Berg C., Rayner J. M. V., (1995), "The moment of inertia of bird wings and the inertial power requirement for flapping flight", Journal of Experimental Biology, 198, 1655-64.

[13] Brown R.H.J., (1953), "The flight of birds:II. Wing function in relation to flight spee", The Journal of Experimental Biology, 30, 90–103.

[14] Burger A., Gochfeld M., (1996), "Family Laridae (Gulls)", Handbook of the Birds of the World, Hoatzin to Auks. Barcelona: Lynx Edicions, 3, 572–599.

[15] Cenizo M., Noriega J. I., Reguero M. A., (2016), "A stem falconid bird from the Lower Eocene of Antarctica and the early southern radiation of the falcons", Journal of Ornithology, 157(3), 885–894.

[16] Chen K., Liu Q., Liao G., Yang Y., Ren L., Yang H., Chen X., (2012), "The Sound Suppression Characteristics of Wing Feather of Owl (Bubo bubo)", Journal of Bionic Engineering, 9(2), 192-199.

[17] Clancy L. J., (1975), "Aerodynamics", Pitman Publishing.

[18] Daniel T. G., Abdulrahim M., Lind R., (2010), "Flight Dynamics of a Morphing Aircraft Utilizing Independent Multiple-Joint Wing Sweep", International Journal of Micro Air Vehicles, 2, 91-106.

[19] del Hoyo J, Andy E., Jordi S., (1992),"Handbook of Birds of the World", Lynx Edicions.

[20] Fielding J., (2017), "Introduction to Aircraft Design (Cambridge Aerospace Series)", Cambridge University Press.

[21] Geyer T., Sarradj E., Fritzsche C., (2010), "Measurement of the noise generation at the trailing edge of porous airfoils", Experiments in Fluids, 48, 291–308.

[22] Geyer T., Sarradj E., Fritzsche C., (2013), "Silent Owl Flight: Comparative Acoustic Wind Tunnel Measurements on Prepared Wings", ACTA Acustica United with Acustica, 99, 139–153.

[23] Geyer T., Sarradj E., Fritzsche C., (2014), "Measuring owl flight noise", Inter-noise Australia, 16-19 November.

[24] Halavanis K., Vachtsevanos G., (2014), "Handbook of Unmanned Aerial Vehicles", Springer.

[25] Harrison J.O., (1991), "Encyclopaedia of Animals: Birds", London Merehurst Press, 109–111.

[26] Hedenström A., (1998), "Flight speed of Ross's Gull Rhodostethia rosea and Sabine's Gull Larus sabini", Arctic, 51(3), 283-285.

[27] Hertel H., (1963), "Struktur, Form, Bewegung", Mainz, Germany, Otto Krauskopf-Verlag Mainz.

[28] Hosder S., Schetz A. J., Mason W. H., Grossman B., Haftka R. T., (2010), "Computational-Fluid-Dynamics-Based Clean-Wing Aerodynamic Noise Model for Design", Journal of Aircraft, 47(3), 754-762.

[29] Howe M.S., (2003),"Theory of Vortex Sound", Cambridge University Press.

[30] Ito S., (2009), "Aerodynamic Influence of Leading-Edge Serrations on an Airfoil in a Low Reynolds Number", Journal of Biomechanical Science and Engineering, 4(1), 117-123.

[31] Kondo K., Aono H., Nonomura T., Oyama A., Fujii K., Yamamoto M., (2013), "Large-Eddy Simulations of Owl-Like Wing Under Low Reynolds Number Conditions", Fluids Engineering Division Summer Meeting, Nevada, USA, 7-11 July.

[32] Kondo K., Aono H., Nonomura T., Oyama A., Fujii K., Yamamoto M., (2014), "Analysis of Owl-like Airfoil Aerodynamics at Low Reynolds Number Flow", Trans. JSASS Aerospace Tech. Japan, 12(29), 35-40.

[33] Konig C., Welck F., Becking J., (1999), "Owls: A Guide to the Owls of the World", Yale University Press.

[34] Kopania J., (2016), "Acoustic parameters: The wings of various owls", Inter-noise, Hamburg, Germany.

[35] Kundu P. K., Cohen I. M., Dowling D. R., (2012), "Fluid Mechanics", 5th Edition, Elsevier.

[36] Lawren L. G., Amin M., Daniel J. I., (2017), "Effects of Speed on Coupled Sweep and Camber in Morphing Wings", 55th AIAA Aerospace Sciences Meeting, Grapevine, Texas, 9-13 January.

[37] Lee M., Cau A., Naish D., Dyke G. J. (2014), "Morphological Clocks in Paleontology, and a Mid-Cretaceous Origin of Crown Aves", Systematic Biology, Volume 63(3), 442-449.

[38] Lentink D., Müller U. K., Stamhuis E. J., de Kat R., van Gestel W., Veldhuis L. L. M., Henningsson P., Hedenström A., Videler J. J., van Leeuwen J. L., (2007), "How swifts control their glide performance with morphing wings", Nature, 446, 1082-1085.

[39] Li D., Liu X., (2016), "Aerodynamic Performance and Acoustic Charaecteristics of Bionic Airfoil Inspired by Three-Dimensional Long-Eared Owl Wing Under Low Reynolds Number", Turbomachinery Technical Conference and Exposition, Seoul, South Korea, 13-17 June.

[40] Liang J., Weiyang Q., Liangfeng W., Fan T., Weijie C., (2014), "Experimental and Numerical Study on Noise Reduction Mechanisms of an Airfoil with Serrated trailing edge", 20th AIAA/CEAS Aeroacoustics Conference, Atlanta, GA, 16-20 June.

[41] Lighthill M.J.,(1652), "On Sound Generated Aerodynamically. I. General Theory", Proceedings of the Royal Society of London. Series A, Mathematical and Physical Sciences, 211(1107), 564-587.

[42] Lilley G. M., (1998), "A study of the silent flight of the owl", AIAA Paper, 1998-2340.

[43] Liu X., Liu X., (2016), "A Numerical Study of Aerodynamic Performance and Noise of a Bionic Airfoil Based on Owl Wing", Hindawi Publishing Corporation Advances in Mechanical Engineering, 6, 1-10.

[44] Livezey B. C., Zusi R. L., (2007), "Higher-order phylogeny of modern birds (Theropoda, Aves: Neornithes) based on comparative anatomy. II. Analysis and discussion", Zool J Linn Soc, 149(1), 1-95.

[45] Mascha E., (1904), "Über die Schwungfedern", Z. Wiss. Zool., 77, 606–651.

[46] Mebs, T., Scherzinger W., (2000), "Die Eulen Europas", Frankh-Kosmos Verlag.

[47] Micael S., Couceiro A., Fonseca F. N. M., Tenreiro M. J. A., (2009), "Application of fractional algorithms in the control of a robotic bird", Communications in Nonlinear Science and Numerical Simulation, 15(4), 895-910.

[48] Mikkola H., (1983), "Owls of Europe", 2nd edition, A&C Black Publishers Ltd.

[49] Nachtigall W., Wieser J., (1966), "Profilmessungen an Taubenflügeln", Zentralblatt für vergleichende Physiologie, 52, 333-346.

[50] Neuhaus W, Bretting H, Schweizer B., (1973), "Morphologische und funktionelle Untersuchungenu¨ber den ‘lautlosen’ Flug der Eulen (Strix aluco) im Vergleich zum Flug der Enten (Anas platyrhynchos)", Biol. Zbl, 92, 495–512.

[51] Norton M.P., Karczub D.G. (2003),"Fundamentals of Noise and Vibration Analysis for Engineers", Cambridge University Press.

[52] Parslew, B. And William J. Crowther., (2010), "Simulating Avian Wingbeat Kinematics", Journal of Biomechanics, 43, 3191–3198.

[53] Pope S., (2000), "Turbulent Flows", Cambridge University Press.

[54] Powell A., (1964), "Theory of Vortex Sound", The Journal of the Acoustical Society of America, 36(1), 177.

[55] Rao C., Ikeda T., Nakata T., Liu H., (2017), "Owl-inspired leading-edge serrations play a crucial role in aerodynamic force production and sound suppression", Bioinspiration & Biomimetics, 12(4).

[56] Riccardo Niccoli, (2013), "History of Flight: From Leonardo's Flying Machine to the Conquest of Space", White Star Publishers.

[57] Roeser R., Valente M., (2007), "Audiology: Diagnosis", Thieme.

[58] Roskam, J., Lan C. T., (1997), "Airplane aerodynamics and performance", Lawrence: Design, analysis and research cooperation.

[59] Sale R., (2016), "Falcons", Collins New Naturalist Library, Harper Collins UK.

[60] Sarradj E., Fritzsche C., Geyer T., (2011),"Silent Owl Flight: Bird Flyover Noise Measurements", AIAA Journal, 49(4), 769-779.

[61] Schwind RG, Allen HJ., (1973), “The effects of leading edge serrations on reducing flow unsteadiness about airfoils”, AIAA Paper , 89.

[62] Shannon C. E., (1949), "Communication in the presence of noise", Proceedings of the Institute of Radio Engineers. 37(1), 10–21.

[63] Theodore M., Scherzinger W., (2000), "Die Eulen Europas: Biologie, Kennzeichen, Bestände", Kosmos Naturführer.

[64] "The Speed of Animals", (2003), The New Book of Knowledge, Grolier Academic Reference, 278.

[65] Tianshu L., Kuykendoll K., Rhew R., Jones S., (2006), "Avian Wing Geometry and Kinematics", AIAA Journal, 44(5), 954-963.

[66] Tobalske B. W., (2007), "Biomechanics of bird flight", The Journal of Experimental Biology, 210, 3135-3146.

[67] Tobalske B. W., Kenneth P. D., (1996), "Flight Kinematics of Black-Billed Magpies and Pigeons Over A Wide Range of Speeds", The Journal of Experimental Biology, 199, 263–280.

[68] Tobalske B., Peacock W. L., Kenneth P. D., (1999), "The intermittent flight of Zebra Finches: Unfixed gears and body lift", Journal of Experimental Biology, 202, 1725-39.

[69] Tucker V. A., (1992), "Pitching Equilibrium, Wing Span and Tail Span in a Gliding Harris' Hawk, Parabuteo Unicinctus", Journal of Experimental Biology, 165, 21-41.

[70] Tucker V. A., Parrott G. C., (1970), "Aerodynamics of Gliding Flight in a Falcon and Other Birds", Journal of Experimental Biology, 52, 345-367.

[71] United States Civil Aeronautics Administration, (1947), "A selected and annotated bibliography of recent air age education textbooks", U.S. Dept. of Commerce, Civil Aeronautics Administration, Office of Aviation Training.

[72] Vad J., Kosco G., Gutermuth M., Kasza Z., Tabi T., Csörgö T., (2006), "Study of the Aero-Acoustic and Aerodynamic Effects of Soft Coating upon Airfoil", JSME International Journal, Series C, 49(3), 648-656.

[73] Weger M., Wagner H., (2016), "Morphological Variations of Leading-Edge Serrations in Owls (Strigiformes)", PLoS ONE, 11(3), e0149236.

[74] Weiyang Q., Liang J., Kunbo X., Weijie C., Fan T., (2013), "An Investigation on the near-field turbulence and radiated sound for an airfoil with trailing edge serrations", 19th AIAA/CEAS Aeroacoustics Conference, Berlin, Germany, 27-29 May.

[75] White, C.M., (1994), "Family Falconidae", In del Hoyo J., Elliot, A., Sargatal J. (eds.), Lynx Edicions, 216–275.

[76] Williams J.E.F., Hawkings D.L.,(1968),"Sound Generation by Turbulence and Surfaces in Arbitrary Motion", Philosophical Transactions of the Royal Society of London, Series A, Mathematical and Physical Sciences, 264(1151), 321-342.

[77] Winzen A., Roidl B., Schröder W,. (2016), "Combined particle-image velocimetry and force analysis of the three-dimensional fluid–structure interaction of a natural owl wing", Bioinspiration & Biomimetics, 11(2), e026005.

[78] Wolf T., Konrath R., (2015), "Avian wing geometry and kinematics of a free-flying barn owl in flapping flight", Experiments in Fluid, Springer Berlin Heidelberg.

[79] Yavuz K., Sermet Ş., Yılmaz Ö., (1971), "Havacılık tarihinde Türkler", Hava Kuvvetleri Basım ve Neşriyat Müd.

BIOGRAPHY

Ferit YILDIZ was born on April 1993, in Duisburg/Germany. His bachelor's degree from University of Kocaeli between 2011-2016, was completed in Mechanical Engineering, with a six month study as an erasmus exchange student at Technical University of Chemnitz. After that, he completed his postgraduate education at Gebze Technical University, Institute of Science and Technology, Department of Mechanical Engineering between 2017-2020. During his undergraduate education, in 2012 he started his career as a Design & Manufacturing Support Engineer in Pivasis Mühendislik. After working here until 2015, he switched to Mercedes-Benz Türk in 2015, as a Project Assistant Engineer. After his undergraduate education he started again in Pivasis Mühendislik as a Design & Manufacturing Engineer. After that he continued his career in Teknokauçuk A.Ş. – R&D Engineer (2017), AVL Turkey – Battery Design Engineer (2018), and FEV Turkey – Battery Design Engineer (2019), where his career continues until now.

APPENDICES

Appendix A: Publications in the Scope of the Thesis Study

Yıldız F., Tokgöz S., (2019), "Farklı Ses Seviyeleri ile Uçan Kuşların Kanat Profillerinin Aerodinamik Olarak İncelenmesi", GTÜ FBE Lisansüstü Araştırmalar Sempozyumu, Kocaeli, Turkey, 17-18 June.